REVERSE MONTE CARLO MODELING OF METAKAOLIN AND METAKAOLIN-BASED GEOPOLYMER

by

Serhat Arca

B.S., Chemical Enginering, Boğaziçi University, 2013

Submitted to the Institute for Graduate Studies in
Science and Engineering in partial fulfillment of
the requirements for the degree of
Master of Science

Graduate Program in Chemical Engineering
Boğaziçi University
2016

ACKNOWLEDGEMENTS

Firstly, I would like to thank my supervisor Assist. Prof. Sezen Soyer Uzun for her patience and support throughout my study.

I also want to thank my colleagues Ramazan Oğuz Canıaz, Refika Çetintaş, Emel Başkent and Elif Kocaman for their help and patience during my study. I express thanks to my friends Coşar Doğa Demirhan, Barış Burnak, Meltem Baysal, Sinem Nalbant, Sevi Hasdemir and Cansu Seçkin for their help and support.

I am very grateful to my family for their support throughout my life. They always contributed to my success and helped me with everything.

I would like to acknowledge Chris J. Benmore for carrying out the high- energy x-ray diffraction measurements. This research used resources of the Advanced Photon Source, a U.S. Department of Energy (DOE) Office of Science User Facility operated for the DOE Office of Science by Argonne National Laboratory under Contract No. DE-AC02-06CH11357.

I also would like to acknowledge TUBITAK BIDEB scholarship program and Boğaziçi University Research Fund (Project BAP13A05P5) for supporting my thesis studies.

ABSTRACT

REVERSE MONTE CARLO MODELING OF METAKAOLIN AND METAKAOLIN- BASED GEOPOLYMER

A metakaolin-based geopolymer with an approximate composition of $NaAlSi_2O_6.5.5H_2O$ is synthesized by mixing metakaolin powder with a $Na_2Si_3O_7$/NaOH solution at ambient conditions. High-energy x-ray diffraction data are collected for kaolinite, metakaolin and the geopolymer at the Advanced Photon Source (APS) in Argonne National Laboratory.

The data is initially used to study the structural changes during dehydroxylation of kaolinite to metakaolin. The radial distribution functions show that the nearest-neighbor Al coordination environment changes from ochahedral to mainly tetrahedral form with calcination.

Reverse Monte Carlo (RMC) modeling is employed to generate realistic three-dimensional models of metakaolin and geopolymer systems based on experimental high-energy x-ray diffraction data. The RMC model of metakaolin indicated that the Al and Si layers in the kaolinite structure is somewhat preserved after dehydroxylation, although greatly distorted. The interlayer distance between Al and Si layers in metakaolin is found to be 3.1 Å. RMC model of the geopolymer, on the other hand, resulted in a three-dimensional structure consisting of randomly cross-linked AlO_4 and SiO_4 tetrahedral units. The bond angle distributions obtained from this model is found to be comparable to leucite mineral. A ring size distribution analysis performed on the system revealed that intermediate-range order in $NaAlSi_2O_6.5.5H_2O$ geopolymer system mainly consist of 7 and 8 membered rings together with considerable amount of 6 membered rings. When the results for the geopolymer model are compared to those for minerals that are considered as analogs to geopolymer structure, namely leucite, nepheline and analcime, it is seen that a much wider variety of ring sizes exists in geopolymer structure compared to these minerals.

ÖZET

METAKAOLİN VE METAKAOLİN BAZLI JEOPOLİMERLERİN REVERSE MONTE CARLO YÖNTEMİ İLE MODELLENMESİ

Metakaolin ve $Na_2Si_3O_7$/NaOH çözeltileri kullanılarak yaklaşık kompozisyonu $NaAlSi_2O_6.5.5H_2O$ olan jeopolimer oda koşullarında sentezlenmiştir. Kaolin, metakaolin ve jeopolimer için yüksek enerjili x-ışını kırınım verisi Argonne Ulusal Laboratuvarında elde edilmiştir.

Elde edilen bu veriler öncelikle kaolinin metakaoline kalsinasyonu sırasında meydana gelen yapısal değişikliklerin tespit edilmesi amacıyla kullanılmıştır. Radyal dağılım fonksiyonları incelendiğinde, kalsinasyon öncesinde altı olan Al atomunun koordinasyon numarasının çoğunlukla dörde dönüştüğü tespit edilmiştir.

Metakaolin ve jeopolimer sistemleri için üç boyutlu modellerin elde edilmesi amacıyla yüksek- enerjili x-ışını verileri ile Reverse Monte Carlo (RMC) modelleme yöntemi kullanılmıştır. Metakaolin için elde edilen RMC modelinde, kaolinin yapısında görülen Al ve Si katmanlarının kalsinasyon sonrasında halen korunduğu; ancak katmanlarda bozulmaların meydana geldiği tespit edilmiştir. Metakaolin yapısında Al ve Si katmanları arasındaki mesafe 3.1 Å olarak belirlenmiştir. Jeopolimerin RMC modeli incelendiğinde ise, jeopolimerin birbirine çapraz bağlı AlO_4 ve SiO_4 tetrahedral ünitelerden oluştuğu gözlenmiştir. Oluşturulan bu model kullanılarak elde edilen bağ açısı dağılımının mineral lösit ile benzer olduğu belirlenmiştir. $NaAlSi_2O_6.5.5H_2O$ jeopolimerinin orta- ölçekteki düzeninin belirlenmesi amacıyla yapılan halka boyutu dağılımı analizi sonuçlarına göre, jeopolimerin çoğunlukla 7 ve 8 halkalı AlO_4 ve SiO_4 tetrahedral ünitelerden oluştuğu, bunun yanında önemli bir miktarda 6 halkalı yapıların jeopolimer yapısında bulunduğu tespit edilmiştir. Jeopolimer için elde edilen sonuçlar, jeopolimer yapısına analog olarak kabul edilen minerallerle, lösit, nefel ve analsim, kıyaslandığında, jeopolimer yapısında bu minerallere kıyasla çok daha geniş bir aralıkta halkalı yapıların bulunduğu görülmüştür.

TABLE OF CONTENTS

LIST OF FIGURES

LIST OF TABLES

1. INTRODUCTION

Traditionally, Portland Cement has been the most commonly used binder material in concrete. However, it has a high carbon dioxide equivalent, ranging between 0.66 and 0.82 kg of carbon dioxide per kg of cement produced [1, 2]. With this carbon dioxide equivalent value, cement production is responsible for approximately 5-7% of global CO_2 emissions [2]. With the increasing concern for nature, an alternative binder, called "geopolymer" has started to be considered as a substitute for Portland Cement [3]. It is estimated that usage of geopolymers might decrease CO_2 emissions significantly compared to Portland Cement with some studies reporting 80% reduction [4, 5].

Davidovits was the first person to use the term "geopolymer". He described geopolymers as aluminosilicates formed by polycondensation of alumina and silica rich source materials [6]. Construction and building materials are considered as the main application areas for the geopolymers [7]. In addition to their excellent mechanical properties, geopolymers are known to have fire and chemical resistant properties. These properties make geopolymers useful in different applications. For example, geopolymers could be used as fire resistant coatings on metal and concrete due to their fire resistant properties [8]. There are studies reporting acid resistant behavior of geopolymers as well [9].

In his work, Davidovits explains that during geopolymerization reactions, alumino-silicate oxides (Al^{+3} in 4-fold coordination) react with alkali polysilicates, which results in Si-O-Al bonds. Amorphous to semi-crystalline silico- aluminate structures, such as Poly(sialate) type (-Si-O-Al-O-), Poly(sialate-siloxo) type (-Si-O-Al-O-Si-O-) and Poly(sialate-disiloxo) type (-Si-O-Al-O-Si-O-Si-O-), are obtained after the geopolymerization reaction [10].

Most waste materials contain reactive alumina and silica, which make them good candidates to be used as raw materials in geopolymerization reactions. Previously, many Al-Si containing materials such as fly ash, furnace slag and metakaolin were used as raw materials for the synthesis of geopolymers [11-13] Comparison of the results for these

studies reveals that the properties and microstructure of the geopolymers depend on the raw materials and the processing conditions**.**

Since physical properties of materials are closely related to their atomic structures, it is very important to study the atomic and microstructures of the materials to get a better understanding of the reasons for having certain properties, such as mechanical strength.

The microstructure and micromorphology of geopolymers are characterized mainly by X-Ray Diffraction (XRD), Fourier Transform Infrared Spectroscopy (FTIR) and microscopic investigations.

In their work, Duxson *et al*. synthesized metakaolin-based geopolymers with Si/Al ratios ranging between 1.15 and 2.15, and they used Scanning Electron Microscopy (SEM) analysis to investigate the relation between mechanical strength and microstructures. They observed highly porous microstructures for Si/Al ratios < 1.40. The strength of geopolymers was found to be maximized at a Si/Al ratio of 1.90 [14].

Panias *et al*. investigated the effects of water, sodium hydroxide and sodium silicate contents on the mechanical strength of fly-ash based geopolymers. XRD and FTIR studies were carried out to understand the microstructure of the geopolymers and they aimed to correlate the microstructure with mechanical properties. In their XRD studies they observed major crystalline phases of fly ash and formation of an amorphous phase in the geopolymer structure [15].

In their study, Xu and van Deventer selected three industrial materials, namely fly ash, kaolinite and albite, and studied different combinations of these materials in geopolymerization. It is claimed that this study is different from most of the previous studies because in previous studies, single or bi-component systems were mostly used because of the complexity of the raw materials. The results of the study show that, with the three component system, higher compressive strength values can be obtained. The higher compressive strength values are attempted to be explained with the microstructure of the synthesized geopolymers. In the SEM image of the system, it was observed that kaolinite

was fully transferred into the gel phase whereas partially unreacted fly ash and albite particles were present in the system. The unreacted albite particles act as a reinforcing agent in the geopolymer, which could explain the higher compressive strength results [16].

Solid state nuclear magnetic resonance (NMR) spectroscopy is a widely used technique for determination of the nearest and next nearest neighbor environment in geopolymers. For detailed studies about the structures of silicates and aluminosilicates, high resolution ^{29}Si and ^{27}Al magic angle spinning NMR is a very valuable technique [17]. With ^{29}Si NMR, different cross linked Si tetrahedral units can be distinguished and it is a sensitive technique for determination of the substitution of Al for Si tetrahedral by the characteristic ^{29}Si line shifts [18].

In 1980's, Davidovits used NMR spectroscopy to study the structure of metakaolin-based geopolymers for the first time in literature [19]. In his work, Davidovits carried out ^{27}Al magic-angle spinning nuclear magnetic resonance (MAS NMR) investigations of metakaolin- based geopolymers and observed a chemical shift in the range of 55 ppm, which means that Al is tetrahedrally coordinated in the system [10].

In their study, Barbosa *et al*. found that reaction of aluminosilicate with alkali polysilicates results in polymeric Si-O-Al three-dimensional structures. They also revealed that during geopolymerization reactions, IV, V and VI coordinated Al in the metakaolin changes into IV coordinated Al in the geopolymer network [20].

In their study, Singh *et al*. used ^{29}Si and ^{27}Al MAS NMR in order to get an understanding of the structural details of geopolymer. Their investigation with ^{27}Al MAS NMR showed that transient aluminum species are formed during the reaction of metakaolin with NaOH. Similar to the observations by Barbosa *et al*. [20], they observed that, during geopolymerization reaction, the coordination of aluminum changes from IV,V and VI to IV. In addition to these, the effect of alkalinity on the geopolymerization was studied and it was found that high alkalinity results in poor polymerization. On the other hand, at low alkalinity they observed a ^{29}Si resonance line, which is a result of unreacted metakaolin [18].

In their study, Duxson *et al*. used ^{29}Si MAS NMR to characterize short- range ordering in terms of T-O-T bonds (where T is either Al or Si). Their study revealed that a more random Si/Al distribution is obtained with potassium geopolymers, compared to mixed-alkali and sodium geopolymers [21].

Pair distribution function (PDF) analysis that relies mainly on high-energy x-ray or neutron diffraction is a widely used and informative technique to study the local atomic structure of complex materials [22]. This method makes use of both Bragg and diffuse scattering, which allows one to obtain information about local structure, that cannot be obtained in conventional methods, such as Rietveld refinement [23]. There are several studies that make use of PDF analysis in geopolymer binders. In their work, White *et al*. used PDF analysis to investigate the amount and nature of the water molecules within metakaolin geopolymer [23]. In another work, White *et al*. illuminated the local structural correlations of metakaolin-based geopolymers by in situ neutron PDF analysis [24]. Bell *et al*. investigated the short to medium range structural order of metakaolin- based geopolymer by X-ray atomic PDF technique and compared the results to zeolitic tetragonal leucite. They found that the structural order of geopolymer resembled corner-sharing, silica- based glassy systems [25]. White *et al*. used in situ X-ray total scattering measurements and PDF analysis to investigate the extent of reaction as a function of time for geopolymerization reactions [4]. Bell *et al*. employed X-ray PDF technique to study the short to medium range atomic structure of Cs based geopolymer. They observed that the structural ordering of the Cs geopolymer is similar to cubic pollucite that is obtained after heating the geopolymer [26]. Meral *et al*. also studied the geopolymer structure using PDF analysis and found that their geopolymers resembled zeolitic nepheline in the short- range region [27].

Studies show that information about the nearest neighbor environment in geopolymers can be obtained with mainly PDF analysis (high- energy x-ray diffraction) and solid state nuclear magnetic resonance spectroscopy. Geopolymer structure, at short-length scale, consists of cross-linked AlO_4 and SiO_4 tetrahedral units. However, solid information regarding intermediate-range order in this system is lacking to date. Therefore, a need for a three dimensional model that could reveal beyond nearest neighbor environment and the details of nano-scale ordering in amorphous geopolymer systems arises [28].

In this study, a geopolymer ($NaAlSi_2O_6.5.5H_2O$) is synthesized using metakaolin which is obtained by calcination of kaolinite at 700°C. High- energy x-ray diffraction experiments are performed on kaolinite, metakaolin and geopolymer samples at the Advanced Photon Source, Argonne National Laboratory. Experimental structure factors and pair distribution functions of kaolinite and metakaolin are compared to observe the effects of calcination in structure. Reverse Monte Carlo (RMC) modeling technique is then used to obtain three-dimensional structural pictures of metakaolin and the geopolymer that are consistent with the experimental diffraction data. The obtained structural models are used to elaborate on the intermediate- range order in the geopolymer system.

2. EXPERIMENTAL AND MODELING TECHNIQUES

2.1. Geopolymer Synthesis

Geopolymer synthesis involves mixing metakaolin powder with the activating solution thoroughly. Metakaolin is obtained by calcining kaolinite ($Al_2Si_2O_5(OH)_4$) at 700 °C for 1 h [29]. The chemical composition of the metakaolin used here is given in Table 2.1 [29]:

Table 2.1. Chemical composition of metakaolin.

Chemical composition	**Percentage (wt. %)**
SiO_2	56.21
Al_2O_3	41.04
TiO_2	1.15
K_2O	0.46
Fe_2O_3	0.36
CaO	0.09
MgO	0.07
P_2O_5	0.06

Activating solution used in geopolymer synthesis is obtained by mixing sodium silicate ($Na_2Si_3O_7$) solution and sodium hydroxide (NaOH) pellets in proportions that will lead to Si/Al and Na/Al ratios of 2 and 1, respectively in the system. Sodium silicate solution used has a density of 1.401g/ml at 20 °C and consists of %9 Na_2O, 28% of SiO_2 and the rest water. For geopolymer synthesis, necessary amount of metakaolin is taken into a beaker and the activating solution is added. The metakaolin- activating solution mixture is mixed thoroughly. The samples are left for a few hours for resting followed by a heat treatment at 60 °C for one day. The Si/Al and Na/Al ratios were adjusted to be 2 and 1 respectively, since

previous studies indicate that higher compressive strength results are obtained for geopolymers with Si/Al ratio between 1.8-2.2 and Na/Al ratio 0.9-1.2 [30-32].

2.2. High Energy X-Ray Diffraction

Lab-scale X-Ray Diffraction (XRD) is a widely used technique for structural characterization of materials. In X-Ray Diffraction, the measurements are usually carried out in momentum transfer space, Q($Å^{-1}$). The value of momentum transfer vector, Q, is determined by $4\pi\sin\theta/\lambda$, where λ is the wavelength and 2θ is the angle of scattering. Since the maximum value $\sin\theta$ can take is 1, the maximum value of Q is limited by $4\pi/\lambda$. For a standard laboratory instrument involving Cu Kα radiation with a wavelength of 1.54 Å, the maximum Q value obtained is around 8 $Å^{-1}$ [27].

The XRD pattern for a geopolymer sample obtained by a standard laboratory instrument gives a broad peak centered at 27- 29°. Therefore, in order to get an atomic-scale understanding of the geopolymer structure, it is necessary to obtain data at a much wider Q range. This allows one to study both the short and intermediate- range order in amorphous materials, such as geopolymers. High- energy synchrotron sources makes it possible to acquire data at a much wider Q range. High- energy synchrotron sources operate at wavelengths around 0.1 Å, which is much smaller compared to a standard Cu Kα radiation with a wavelength around 1.54 Å, which results in much higher energy and a much wider Q range [27].

In high- energy x-ray diffraction technique, differential scattering cross-section is measured and it is proportional to the structure factor S(Q). The S(Q) can be calculated by adding up the contribution of each atom pair for a system containing more than one type of atom [27]. For a polyatomic system, the equation for S(Q) is given in Equation 2.1:

$$S_X(Q) - 1 = \frac{I_X(Q)}{\left(\sum_i c_i f_i(Q)\right)^2} = \frac{1}{\left(\sum_i c_i f_i(Q)\right)^2} \sum_{i,j} c_i f_i(Q) c_j f_j(Q)\left(S_{ij}(Q) - 1\right) \qquad (2.1)$$

where $I_x(Q)$ is the distinct scattering, c_i is the atomic concentration of atoms of species i, $S_{ij}(Q)$ are the partial structure factors and f_i is the x-ray form factor.

S(Q) can be used to study the system in reciprocal space. The low Q peaks represent the extended range order and the high Q oscillations are observed as a result of local bond distributions. The study of local structure is carried out more easily by Fourier transforming S(Q) into real space. The equation for the total x-ray pair distribution function, G(r) is given in Equation 2.2:

$$G_x(r) = \frac{f_i(Q)f_j(Q)}{(2\pi)^3\rho_o}\int_0^\infty 4\pi Q^2 S_X(Q)\frac{sinQr}{Qr}dQ \qquad (2.2)$$

where ρ_o is the number density (atoms/ $Å^3$).

In this study, high-energy x-ray diffraction experiments are performed in beamline 6-ID-D at the Advanced Photon Source, Argonne National Laboratory by Chris J. Benmore, using an incident photon wavelength of λ=0.12358(6) Å (E=100.329 keV). Samples were loaded into 1.5 mm diameter cylindrical polyimide tubes (Cole Palmer) of wall thickness 50 μm. A NIST crystalline standard CeO_2 powder was used for the sample-detector distance calibration, which was set to 39.3mm. The diffraction data were collected over a Q range of 0.5-26.9 $Å^{-1}$ using a Perkin Elmer (model XRD 1621) amorphous silicon flat plate area detector with a carbon fiber window. The beam size was 0.5x0.5 mm^2 and data was collected for 180 min for each sample. The reduction of the high-energy X-ray data was carried out using the software analysis package FIT2D. Reliable x-ray structure factors S(Q) were collected up to Q= 22 $Å^{-1}$ using the program PDFgetX2 by applying standard corrections [33].

2.3. Reverse Monte Carlo Modeling

In order to get structural representations of disordered materials such as glasses or liquids, the use of computer modeling or simulation can provide important insights [34]. A simple form of the conventional approach to understand the molecular structures can be outlined as follows [28]:

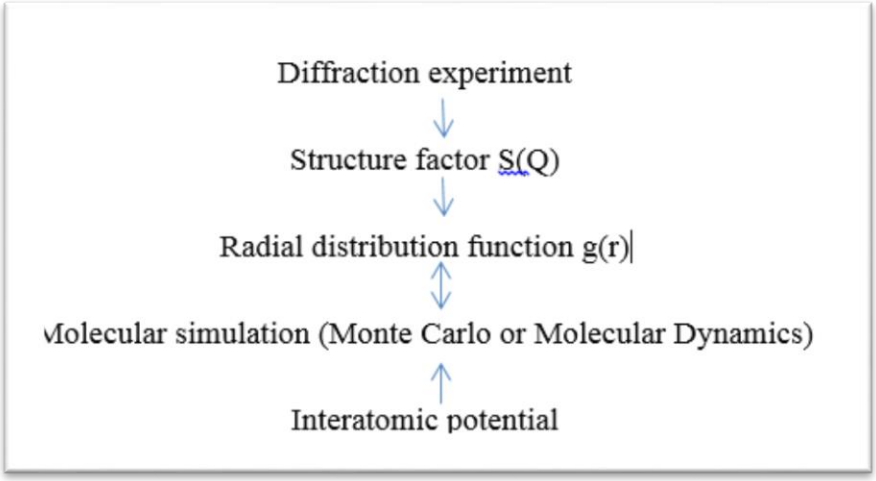

Figure 2.1. Simplified schematic representation of conventional approach for studying molecular structures

Structure factor, S(Q), is obtained after implementation of neutron or x-ray diffraction experiment. The structure factor is Fourier transformed to get radial distribution function, g(r). Molecular dynamics or Monte Carlo simulation technique, which is based on the algorithm developed by Metropolis *et al*. [35], is then used to produce a one dimensional g(r). The g(r) result obtained from the simulation, which is obtained with the help of an interatomic potential, can then be compared with the experimental results [28]. Calculation of an interatomic potential would be very hard for a geopolymer system. Therefore, a simulation method that does not need interatomic potential would be an appropriate choice for studying the geopolymer structure.

Reverse Monte Carlo (RMC) modeling is a technique, which can be used to produce three-dimensional models of a system. RMC modeling has been applied successfully for different types of systems such as liquids, crystals, polymers, glasses and magnetic materials [36]. It is an inverse modeling technique used to generate a structural model by taking the experimental data as an input. The constraints provided to the simulation environment include number density, coordination numbers of the constituent atoms and distances of closest approach between atoms. RMC modeling generates a three dimensional structural model that is consistent with the experimental data. The outputs of the RMC model might include partial structure factors and pair distribution functions [36].

In order to better describe reverse modeling, it is useful to compare it with forward modeling. In forward modeling, an interatomic potential is used to generate atomic configurations. These configurations are used to make calculations and obtain values that can be compared with experimental data. On the other hand, in inverse modeling experimental data is the starting point and atomic configurations are formed such that the obtained atomic configuration gives best agreement with experimental data [37].

The algorithm for Reverse Monte Carlo modeling can be summarized as follows [28]: The subscripts S and E represent simulation and experiment respectively.

- An initial configuration is chosen.
- Periodic boundary conditions are applied and radial distribution function $g_s(r)$, which is the probability to find an atom in the shell dr at a distance r from another particle, is calculated.
- One particle is moved at random to create a new configuration. The new radial distribution function $g'_s(r)$ corresponding to new configuration is calculated.
- $g_s(r)$ is transformed to structure factor $S_s(Q)$ by Equation 2.3

$$S_s(Q) - 1 = \frac{4\pi\rho}{Q} \int_0^\infty r^2 (g_s(r) - 1) \sin Qr \, dr \tag{2.3}$$

- $S_s(Q)$ for two different configurations are compared with the experimental results using a standard χ^2 test as given in Equation 2.4 and 2.5:

$$\chi^2 = \sum_i (S_s(Q) - S_E(Q))^2 / \sigma(Q)^2 \tag{2.4}$$

$$\chi'^2 = \sum_i (S'_s(Q) - S_E(Q))^2 / \sigma(Q)^2 \tag{2.5}$$

- If $\chi'^2 < \chi^2$ the new configuration is accepted. Otherwise, it is accepted with a probability that follows a normal distribution with width σ.
- If the new configuration is accepted, it becomes the new configuration for next step. If it is not accepted, a new configuration is created by the random movement one particle and the same steps are followed.
- The procedure is carried out until χ^2 decreases to an equilibrium value.

RMC modeling has not been used for obtaining three dimensional structures of geopolymers. However, the method has found a wide range of application areas including liquids, polymers, glasses and disorder in crystals [36].

In this study, Reverse Monte Carlo simulations are performed for metakaolin and metakaolin-based geopolymer. RMCA code is used for the simulations [28, 36].

For RMC modeling of raw material metakaolin, the starting configuration is taken from the work by White *et al* [38]. 294 atoms are used in the simulations. Two coordination constraints are given to the system to create AlO_4 and SiO_4 tetrahedras. The number density of metakaolin is calculated as 0.0746 A^{-3} using the specific gravity of metakaolin from the work by Al-Akhras [39]. The experimental S(Q) data is taken from [27]. The cut off distances, which are the bond distances for each of the atom pairs, for the metakaolin model are given in Table 2.2 [25, 40, 41]:

Table 2.2. Cut off distances used in RMC simulations for metakaolin.

	Bond distance (Å)
Al-Al	3.1
Al-Si	3.1
Al-O	1.75
Si-Si	3.1
Si-O	1.62
O-O	2.6

RMC modeling of geopolymer is carried out using 1065 atoms in the simulations. Using the specific gravity of the geopolymer from the work by Sakkas *et al*. [42], the number density is calculated to be 0.09013 A^{-3}. The nearest- neighbor bond distances were obtained from previously published studies and were given as constraints to the simulation [25, 40, 41, 43-48]. The bond distances that are used in the simulations can be seen in Table 2.3:

Table 2.3. Cut off distances used in RMC simulations for metakaolin geopolymer.

	Bond distance (Å)
Al-Al	3.1
Al-Si	3.1
Al-O	1.75
Al-Na	2.8
Al-H	2.38
Si-Si	3.1
Si-O	1.62
Si-Na	3.35
Si-H	2.3
O-O	2.6
O-Na	2.6
O-H	0.99
Na-Na	3.5
Na-H	2.44
H-H	1.42

^{29}Si and ^{27}Al MAS-NMR studies reveal that both Al and Si have four nearest neighbor O atoms [18, 20]. These coordination numbers are given as constraints to the simulation as well.

The first step in the RMC simulation of the geopolymer is randomly placing the atoms inside a cubic cell. Then the atoms are moved to new positions randomly to match with the constraints given to the simulation, such as nearest- neighbor distances and coordination numbers constraints. Following this step, these atomic configurations are used in the RMC simulations in order to match the simulation and experimental x-ray diffraction structure factors.

3. RESULTS AND DISCUSSIONS

3.1. Structural Transformation of Kaolinite into Metakaolin: High- Energy XRD Results

Metakaolin is used as the raw material for geopolymer synthesis. As previously mentioned, it is obtained by dehydroxylation of kaolinite ($Al_2Si_2O_5(OH)_4$) at elevated temperatures. This part of the thesis presents experimental high-energy diffraction results that compare the structures of kaolinite and metakaolin.

In this part, high- energy x-ray diffraction is used to study the structural changes during dehydroxylation of kaolinite to form metakaolin experimentally. The total structure factors of kaolinite and metakaolin are shown in Figure 3.1. It is clearly seen that the highly crystalline nature of kaolinite, evident from the intense sharp features in its structure factor, has evolved into a more disordered form displaying broad features. This type of crystalline to amorphous transformation in this system has been also previously monitored by infrared spectroscopic results [29].

These structure factors (Figure 3.1) are Fourier transformed to obtain total pair distribution functions, G(r) of kaolinite and metakaolin. The results are given in Figure 3.2:

An investigation of Figure 3.2 reveals that G(r) of crystalline kaolinite displays strong correlations up to a distance of 14 Å. On the other hand, metakaolin, dehydroxylated form of kaolinite, exhibits a G(r) with almost no correlations after an r value of 7 Å. It is seen that calcination procedure resulted in a disordered material that is known to be active for geopolymerization.

For a better understanding of the local structure, a zoomed in version of the total pair distribution function results for kaolinite and metakaolin is given in Figure 3.3. The peaks are labeled with respect to the atom pairs that are mainly responsible from these features.

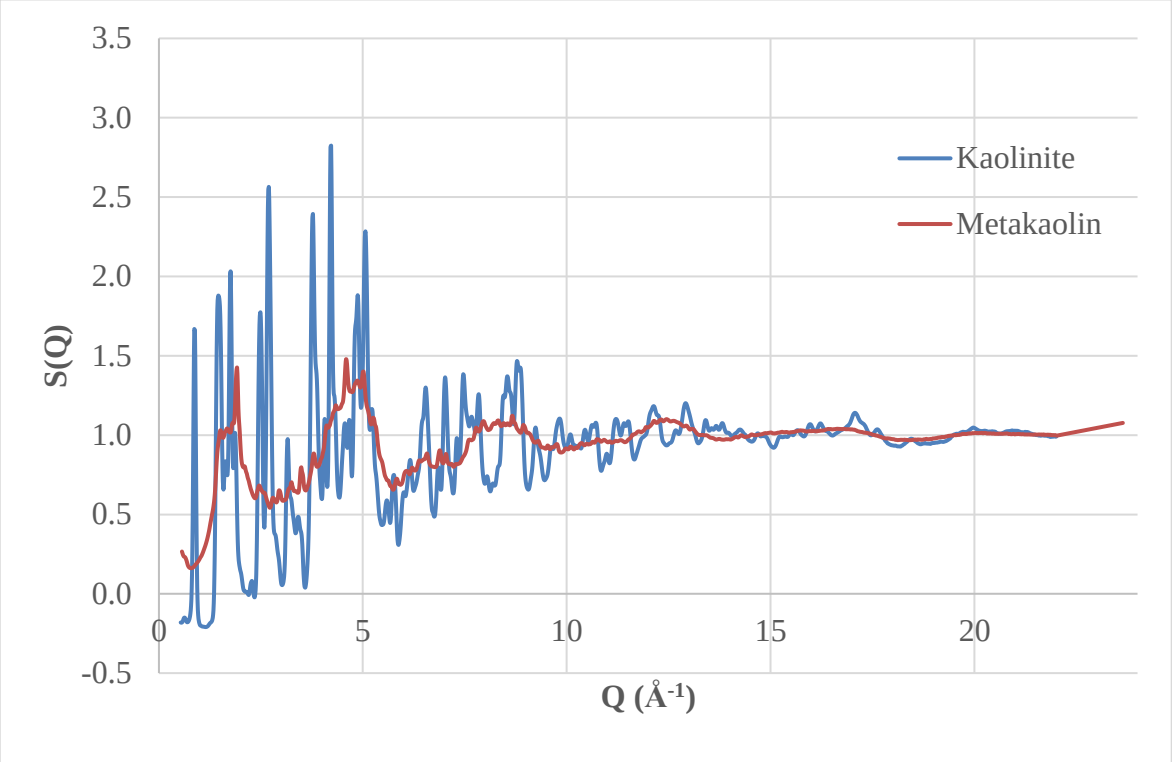

Figure 3.1. Experimental total structure factors for kaolinite and metakaolin.

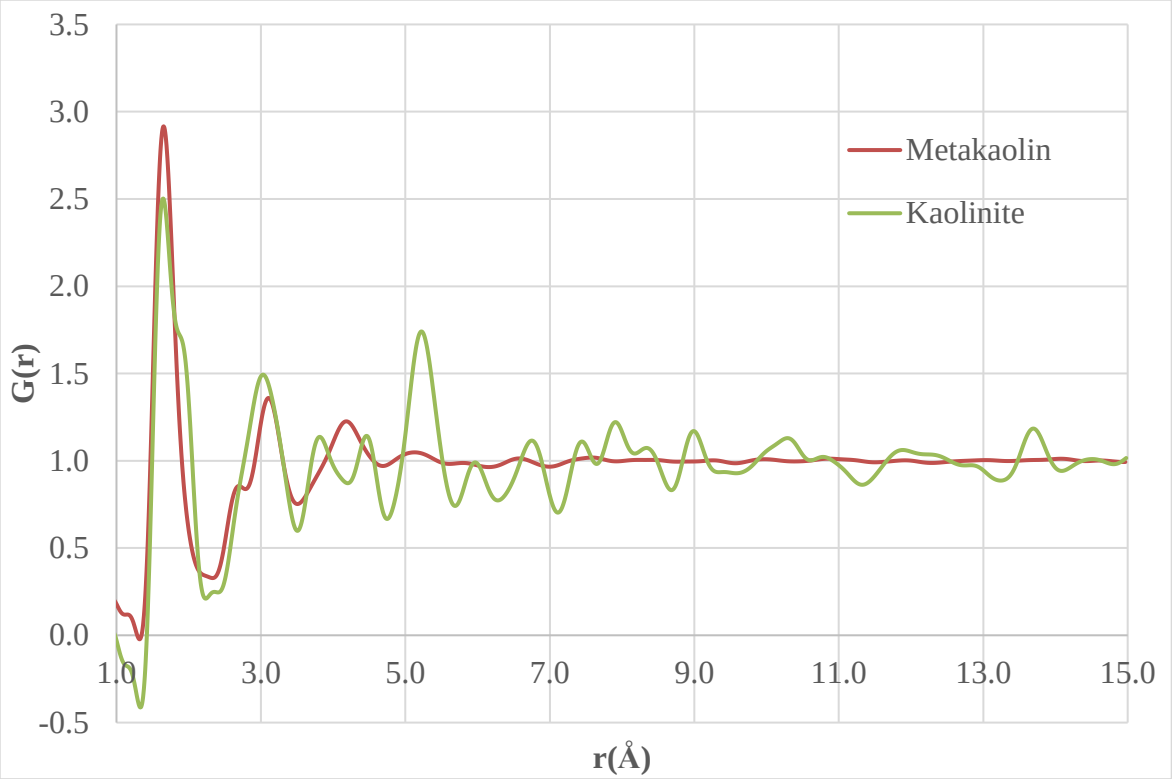

Figure 3.2. Total pair distribution functions for kaolinite and metakaolin.

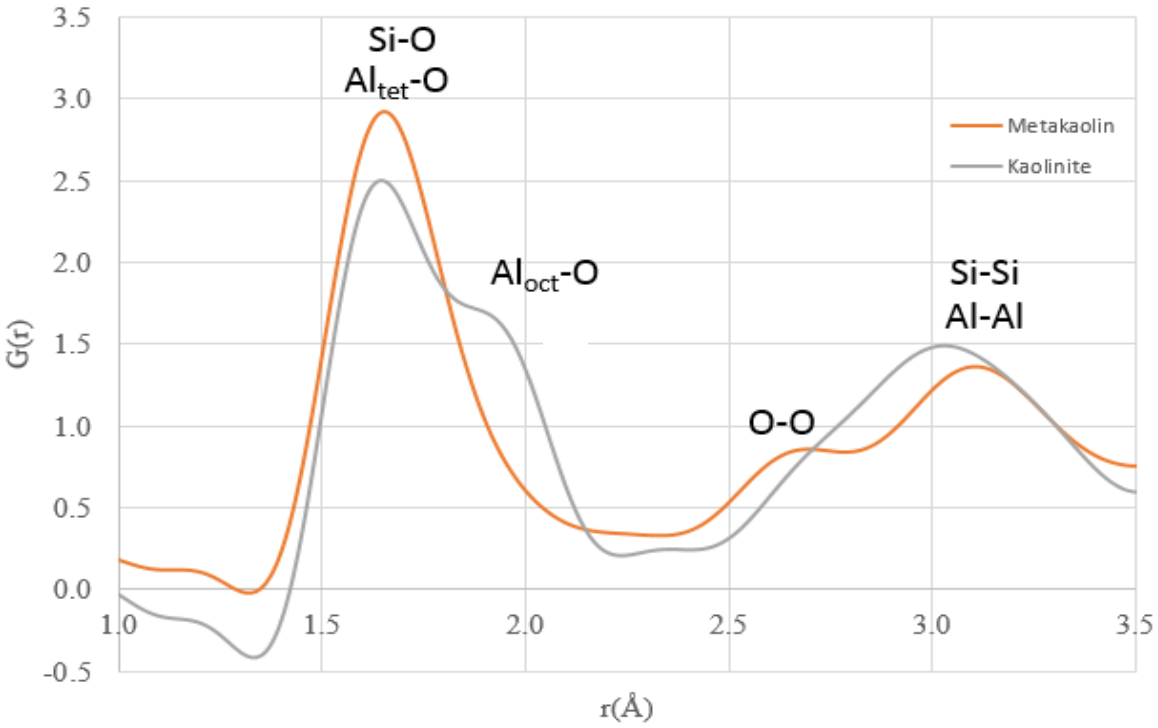

Figure 3.3. Total pair distribution functions for kaolinite and metakaolin in the r region between 1 Å and 3.5 Å.

The nearest neighbor environment in the total G(r) of kaolinite consists of two distinct features positioned at about 1.7 and 1.9 Å. The intense peak at 1.7 Å corresponds to SiO_4 and AlO_4 terahedral units whereas the shoulder positioned at 1.9 Å corresponds to octahedral AlO_6 units. The presence of a shoulder around 1.9 Å in the G(r) of kaolinite is seen as the most striking difference between the radial distribution functions of kaolinite and metakaolin. Octahedral Al-O is responsible for the shoulder around 1.9 Å and as the calcination proceeds, the peak position changes from 1.9 to 1.7 Å, revealing that the octahedral Al-O is converted into tetrahedral Al-O with the calcination process. This observation is in agreement with the results from Sperinck *et al*., where they observed a shift for Al-O peak from 1.93 Å to 1.75 Å as a result of dehydroxylation [49]. Sperinck *et al*. also reported 5-fold Al coordination with the final structure containing around 88% 4-fold coordinated, 11% 5-fold coordinated and 1% 6-fold coordinated Al [49]. The presence of 5-fold coordination is also reported in the work by White *et al*. [50]. In Figure 3.3, a separate peak, which can be attributed to 5-fold Al coordination, is not present. It is probably hidden in the broad peak centered on 1.7 Å. In fact, in their PDF analysis study, Bell *et al*. stated that different coordination environments of Al were not distinguishable in the PDF data [25].

Petkov *et al*. stated that a high resolution (Q~40 $Å^{-1}$) and deconvolution is required to obtain distinguishable data [44]. In addition to these, since, both AlO_4 and SiO_4 tetrahedras are responsible for the peak around 1.7 Å, the intensity of this peak is higher for metakaolin, compared to kaolinite.

Furthermore, the G(r) of metakaolin displays a peak positioned at around 2.6 Å. This peak corresponds to O-O correlations. The O-O correlation in the kaolinite G(r) appears as a minor shoulder at around 2.65 Å. The peak position value of 2.6 Å in the G(r) of metakaolin matches with the value given in the work by Sperinck *et al*. [49]. The peak centered around 3 Å for kaolinite and 3.1 Å for metakaolin corresponds to Al-Al and Si-Si correlations.

3.2. RMC Modeling of Metakaolin and Metakaolin-Based Geopolymer

3.2.1. RMC Modeling of Metakaolin

A three dimensional metakaolin model is obtained by RMC simulations using experimental high-energy diffraction data given in Meral *et al*. [27]. A comparison between the experimental and the RMC generated structure factor, S(Q), can be seen in Figure 3.4:

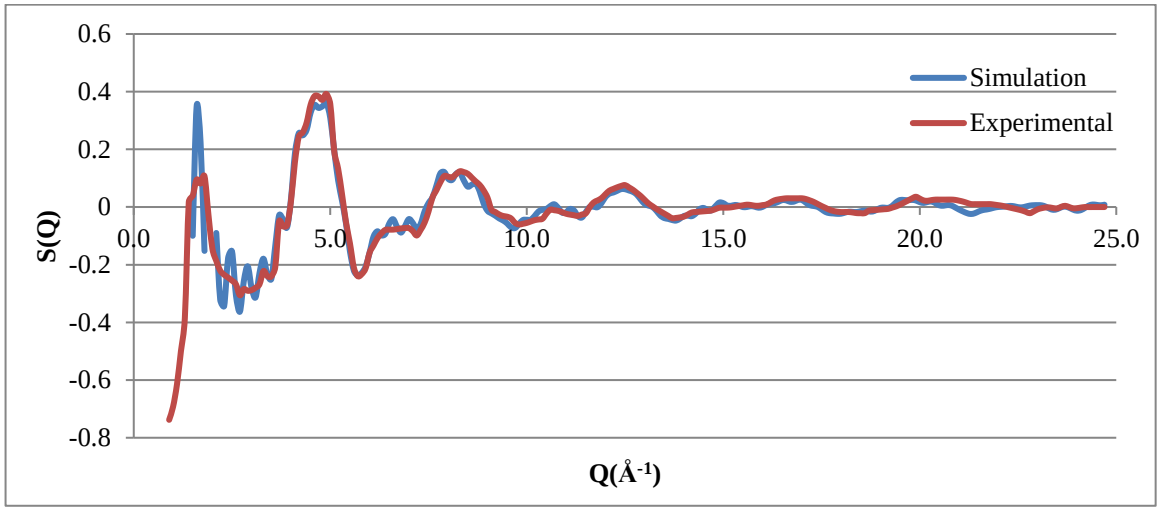

Figure 3.4. Experimental and simulation structure factor for metakaolin.

An investigation of Figure 3.4 shows that the experimental and obtained S(Q) data are in good agreement with a χ^2 value around 230, except for some small fluctuations at low

momentum transfer (Q) values. The agreement between the experimental and simulation S(Q) results shows that the experimental results are duplicated with the obtained model.

The three- dimensional structure of the metakaolin model at the end of the simulation is obtained using GaussView software [51] and is given in Figure 3.5:

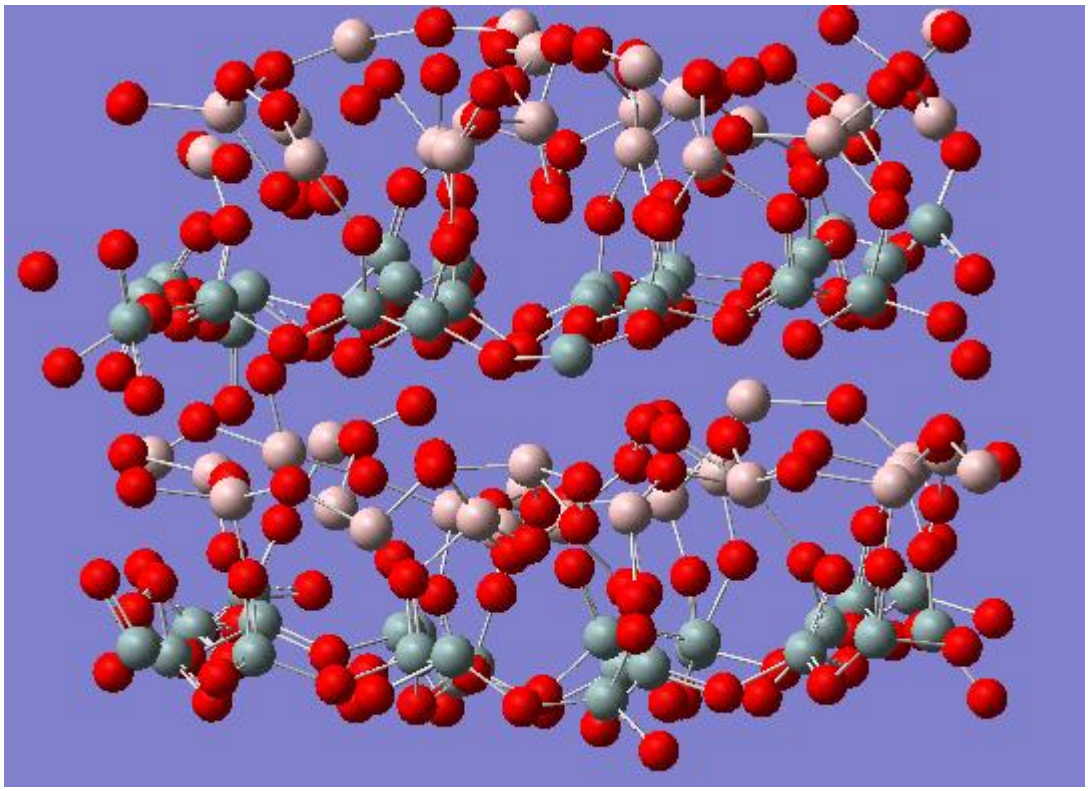

Figure 3.5. 3-D representation of the RMC model of the metakaolin structure. Red, green and pink spheres correspond to O, Si, and Al atoms, respectively.

In Figure 3.5, the red spheres represent oxygen atoms whereas the green spheres are silicon and pink spheres are aluminum atoms. An investigation of Figure 3.5 reveals the distortion in aluminum and silicate layers, which is formed during the dehydroxylation of kaolinite to metakaolin. This observation is in agreement with the work of Sperinck *et al*. and White *et al*. [38, 49]. In their work, Sperinck *et al*. explains that loss of hydroxyls from the structure results in formation of vacancies and these vacancies are responsible for the large distortions in the layers. They further explain that, the distortions takes place because silicon and aluminum atoms leave their positions and move into the interlayer space, which results in formation of bridges between the layers [49].

The short-range order in metakaolin mainly consists of SiO_4 and AlO_4 tetrahedra. In order to further investigate the nearest neighbor environment for the model, the partial g(r) values are obtained based on RMC model and are given in Figures 3.6 -3.11:

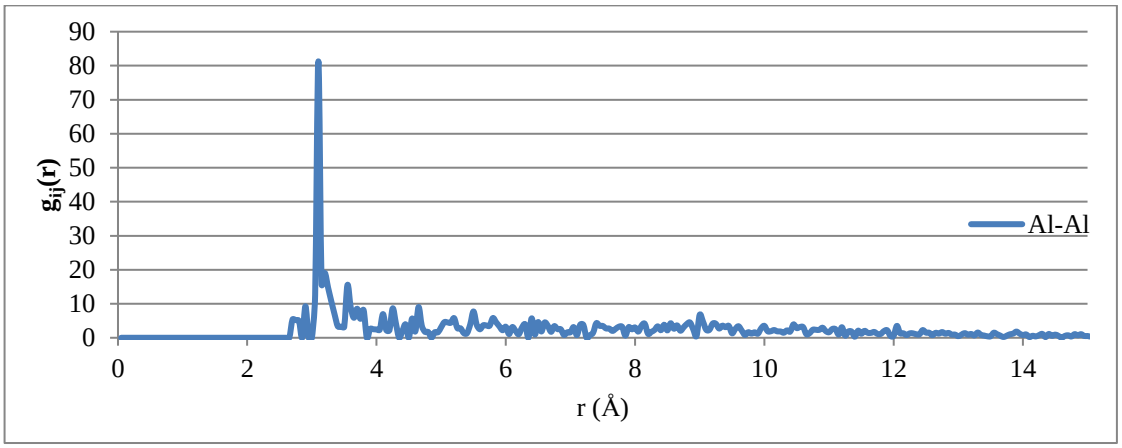

Figure 3.6. Partial pair distribution function results for Al-Al pair in metakaolin model.

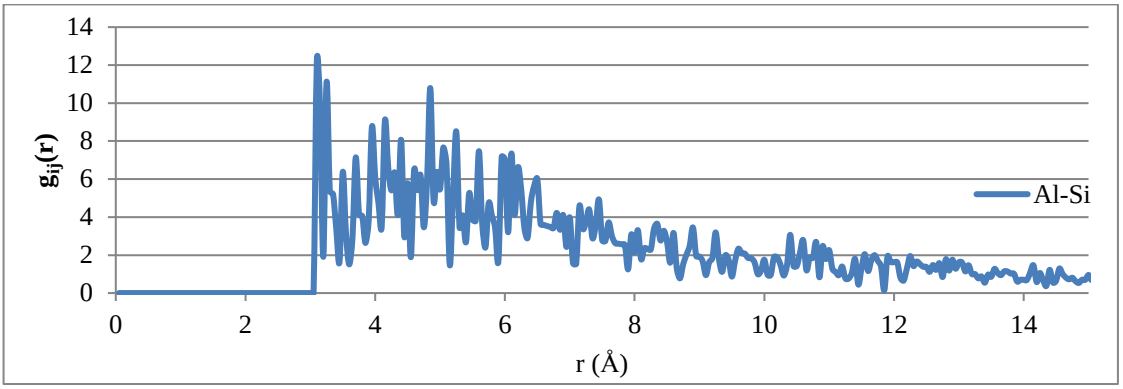

Figure 3.7. Partial pair distribution function results for Al-Si pair in metakaolin model.

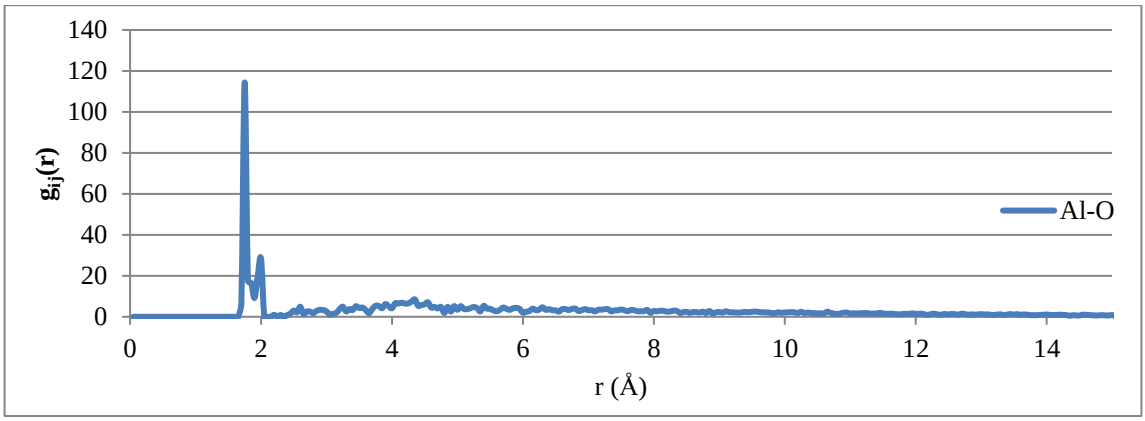

Figure 3.8. Partial pair distribution function results for Al-O pair in metakaolin model.

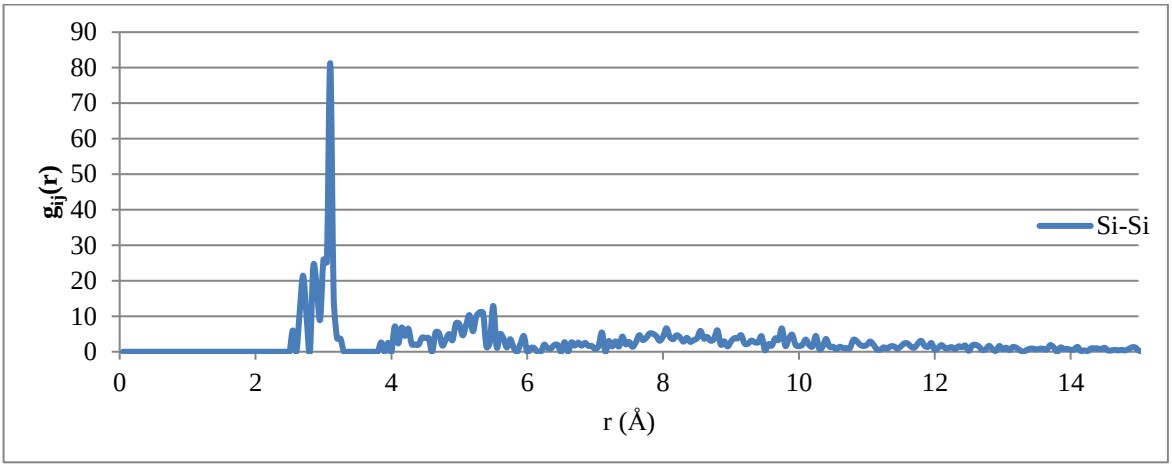

Figure 3.9. Partial pair distribution function results for Si-Si pair in metakaolin model.

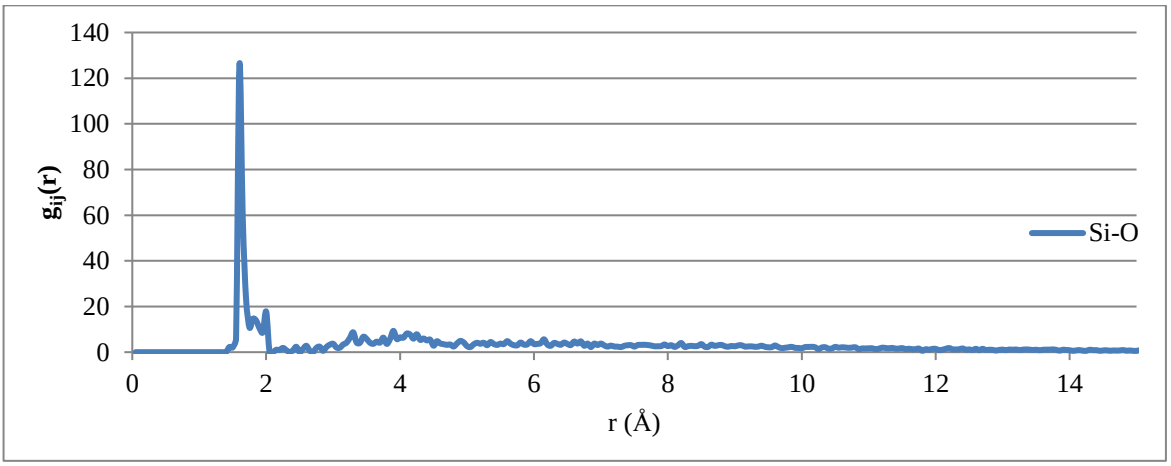

Figure 3.10. Partial pair distribution function results for Si-O pair in metakaolin model.

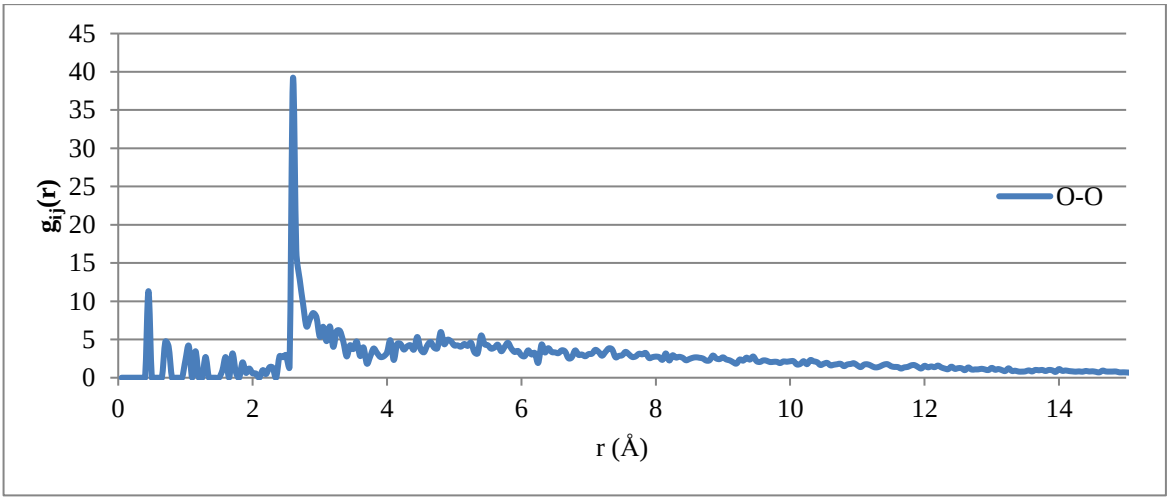

Figure 3.11. Partial pair distribution function results for O-O pair in metakaolin model.

An investigation of the partial pair distribution functions in Figure 3.6- 3.11 reveals that the Al-O, Si-O, and O-O distances are 1.75 Å, 1.6 Å and 2.6 Å, respectively. In their molecular dynamics study of dehydroxylation of kaolinite to form metakaolin, Sperinck *et al*. obtained Si-O peak at 1.68 Å (the experimental value is 1.7 Å), Al-O peak at 1.75 Å and O-O peak at 2.58 Å (experimental value is 2.6 Å) [49]. In this sense, the obtained Al-O and O-O results with the geopolymer model of this study matches with the experimental and previous modeling results. In addition to that, the Si-O result is comparable to the values given in literature.

In addition to the above investigations, the partial pair distribution function results are also used to determine the interlayer distance in the metakaolin structure. Metakaolin is composed of Si and Al layers. Therefore, the Al-Si pair distribution function is observed for this purpose. By using the high intensity peak in the partial pair distribution function of Al-Si pair in Figure 3.6, the Al-Si distance is found to be 3.1 Å. In their work, Sperinck *et al*. obtained the interlayer distance to be between 4.86 a.u. and 6.54 a.u., which corresponds to 2.57 Å and 3.46 Å, respectively and the proposed value is given to be 3.33 Å [49]. A comparison of the obtained result of 3.1 Å with the values given in the work by Sperinck *et al*. reveals that the obtained results are comparable to literature values.

3.2.2. RMC Modeling of Metakaolin-Based Geopolymer

RMC model of metakaolin-based geopolymer is obtained based on the high-energy x-ray diffraction data of this system. 3 coordination constraints were introduced into the RMC model. It is known from previous NMR studies that Al and Si atoms are tetrahedrally bonded to O atoms [10, 18, 20, 21, 52]. These two constraints were used in the simulations along with a constraint that involves bonding of two H atoms to O atoms to form water molecules. The constraints related to AlO_4 and SiO_4 tetrahedra were met around 98% and 96.25%. For the water molecules it is expected that about 47% of the oxygens to be bonded to 2 hydrogens (form water molecules) based on stoichiometry ($NaAlSi_2O_6$ $5.5H_2O$). This constraint is met around 28%.

The experimental S(Q) data supplied to the RMC simulation environment is given in Figure 3.12. The data covers the range from 0.55 to 22 $Å^{-1}$. The S(Q) obtained by RMC modeling is also given in Figure 3.7. It is seen that the experimental and the simulation S(Q) results are in very good agreement, which is also highlighted with a χ^2 value around 50.

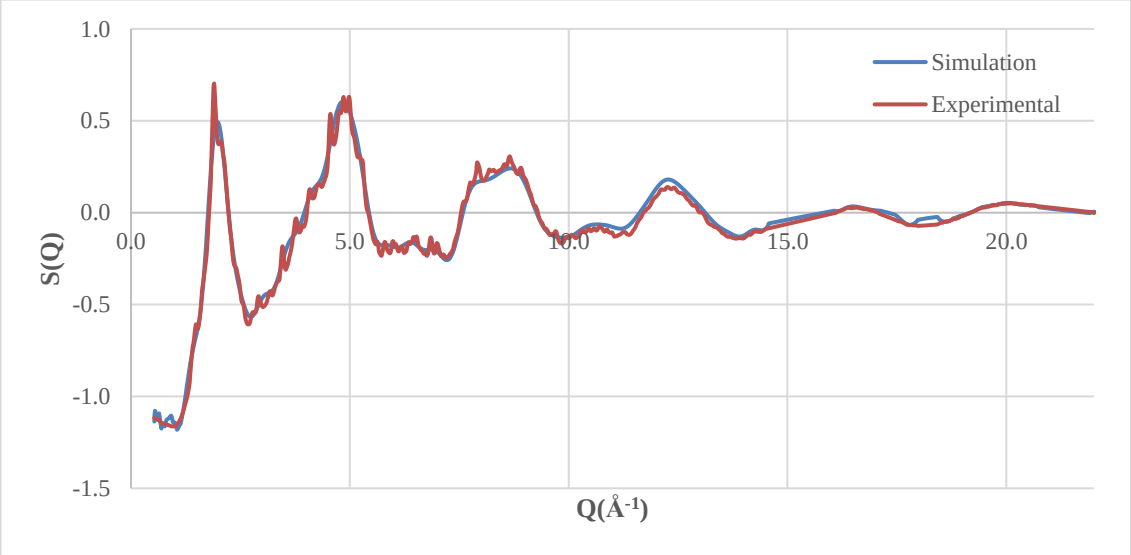

Figure 3.12. Experimental and simulation structure factor for Na-metakaolin geopolymer.

RMC generated 3-D structure for the obtained geopolymer is given in Figure 3.13. In this figure, Red, green, pink, purple, and white spheres correspond to O, Si, Al, Na, and H atoms, respectively.

A comparison of the geopolymer structure in Figure 3.13 with the metakaolin structure in Figure 3.5 reveals that after geopolymerization reactions, the Al and Si layers have disappeared and a more random structure is obtained. The short-range order geopolymer structure consists of AlO_4 and SiO_4 tetrahedral units that are connected to form a network. Sodium atoms seem to be distributed randomly throughout the structure. The intermediate-range order in this system is investigated (Part 3.2.2.3) by the analysis of the presence and size of the rings that are formed by interconnection of these tetrahedral units.

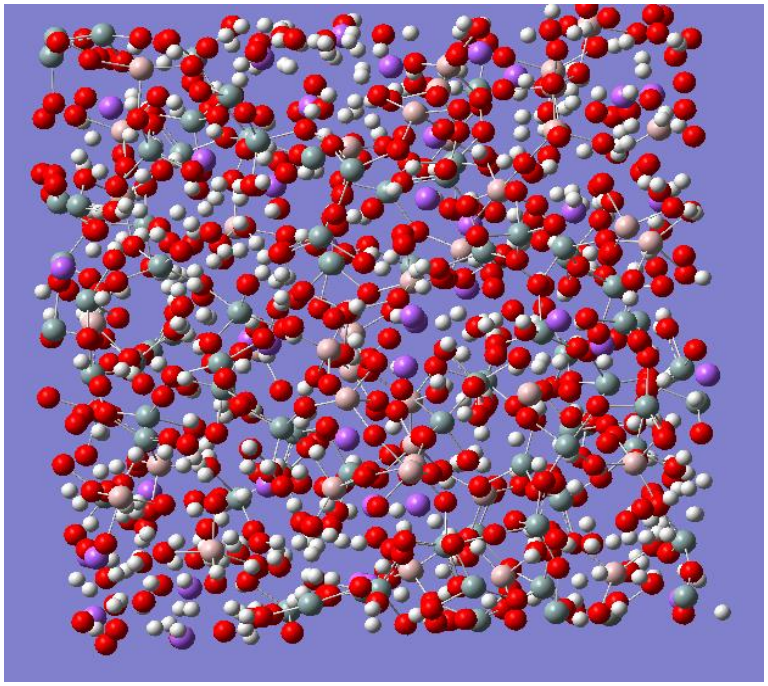

Figure 3.13. 3-D structure for the metakaolin-based geopolymer model. Red, green, pink, purple, and white spheres correspond to O, Si, Al, Na, and H atoms, respectively.

3.2.2.1. Short-Range Order (SRO)

The total pair distribution functions, G(r)'s, are calculated by Fourier Transformation of experimental and simulation S(Q)'s presented in Figure 3.12. A comparison of the total G(r) from the experiment and from the RMC model is given in Figure 3.14:

The x-axis of total G(r) results given in Figure 3.14 is given such that it starts at 1 Å, because there are oscillations in the region between 0 Å and 1 Å. In theory, the limits of the integral in the transformation from S(Q) to G(r) is from zero to infinity. However in reality, it is physically not possible to obtain the upper limit as infinity. The upper limit, in reality is a finite value, Q_{max}, and this results in non-physical oscillations at low r values [53]. In order to eliminate the non-physical oscillations at low r values, the graph is started at 1 Å.

An investigation of Figure 3.14 reveals that the experimental and simulation G(r) are in perfect agreement, in accordance with the S(Q) results given in Figure 3.12.

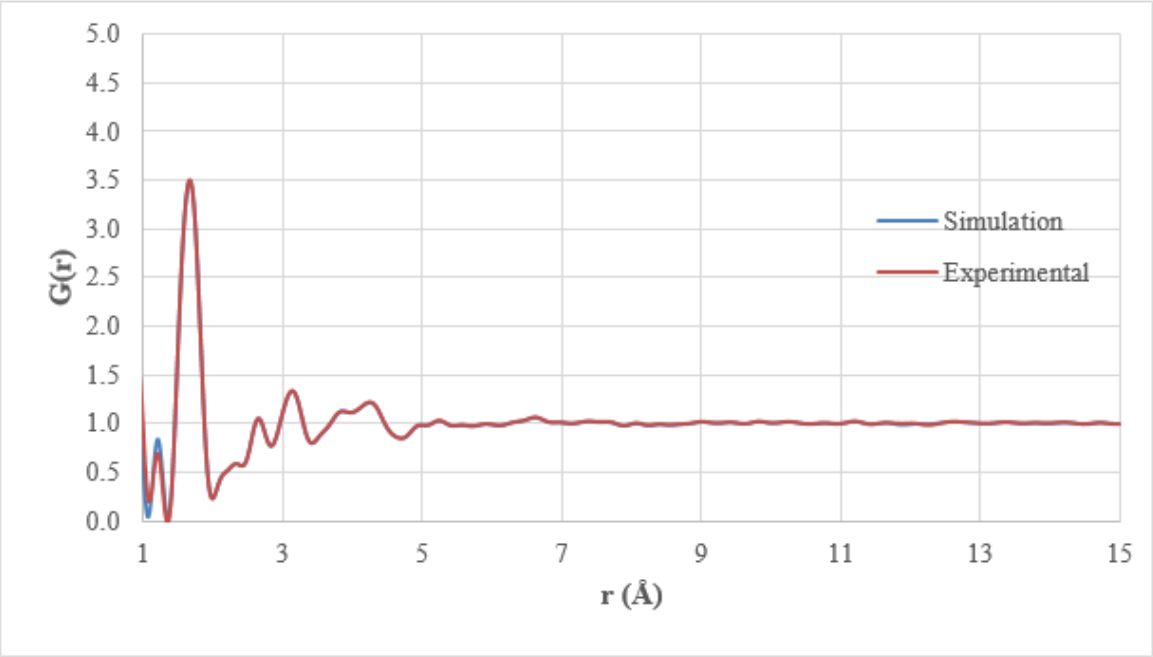

Figure 3.14. Experimental and simulation pair distribution functions for metakaolin-based geopolymer.

For a better study of the local ordering in the geopolymer structure, a zoomed version of the total G(r) that is obtained after simulation is given in Figure 3.15 along with the labels indicating responsible atom pairs for the observed peaks.

The short-range order (until about 4 Å) in geopolymers are reported to be similar to minerals such as leucite ($KAlSi_2O_6$) and nepheline ($KNa_3Al_4(SiO_4)_4$) [27]. Analcime ($NaAlSi_2O_6.H_2O$), in terms of composition, is another mineral that can be used as a reference to compare the structure of geopolymer obtained from RMC modeling. Therefore, short-, and intermediate- range character and bond angle distributions of metakaolin-based geopolymer studied here will be compared with that of leucite, nepheline and analcime.

An investigation of Figure 3.15 in the light of information from literature reveals that the first and sharpest peak around 1.66 Å corresponds to T-O (T: Al, Si) correlations, which agrees well with the literature values [23, 40, 54-63]. The second peak centered on 2.65 Å corresponds to Na-O and O-O correlations.

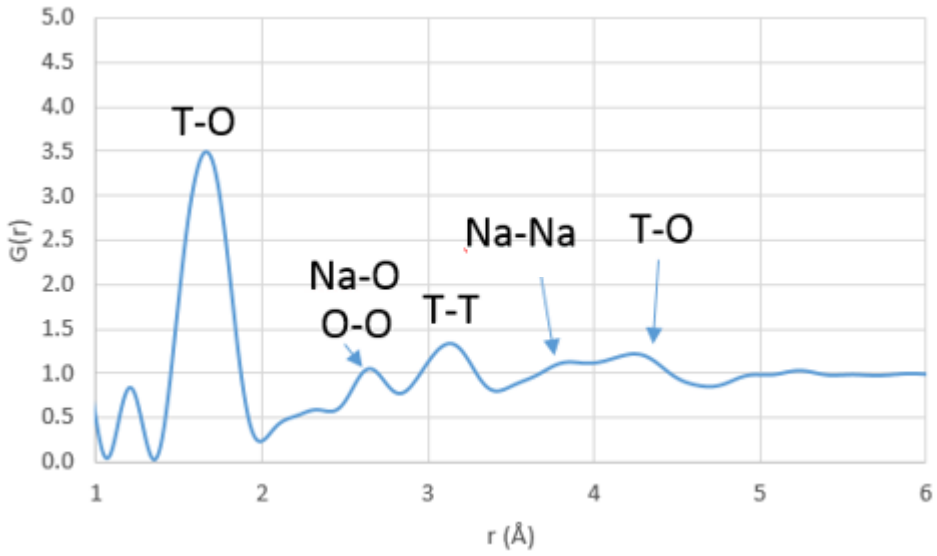

Figure 3.15. G(r) results obtained from RMC model of geopolymer. The peaks are labeled with respect to the atom pairs that are responsible from these features.

The obtained Na-O and O-O distances with the RMC generated geopolymer model is comparable to the values given in [54-58, 60, 62, 63]. T-T correlations contribute to the peak around 3.1 Å in G(r), which is in accordance with the values given in the work by Dove *et al*. [40]. Furthermore, a comparison of the simulation G(r) with the leucite model in the work by Bell *et al*. [25] reveals that the obtained model here and leucite are in good agreement up to ~4 Å except for correlations involving alkali atoms. Bell *et al*. [25] stated that the definite correlations, that are observed up to 4 Å is a sign of well- defined Al and Si polyhedra [25]. Comparison of the total G(r) with the nepheline results given in the work by Meral *et al*. reveals that the results for geopolymer and nepheline are in very good agreement up to ~4 Å. Furthermore, the position of the highest intensity peak for the geopolymer is around 1.7 Å. This position of the peak agrees well with both the geopolymer results presented here and the results of nepheline and leucite given in the work by Bell *et al*. and Meral *et al* [25, 27].

The bond distance results for the geopolymer model are compared to those of the selected minerals. The bond distance results from several studies on the structure of leucite, nepheline and analcime along with the geopolymer model results of this study are given in Table 3.1:

Table 3.1. Bond distances for the RMC model of metakaolin-based geopolymer and selected minerals.

	T-O	**Na-O**	**O-O**	**T-T**
Petkov [44]	1.6			
Meral *et al*. [27]	1.62			
Wyckoff [41]	1.62			
Yokomori and Idaka [54]	1.65	Between 2.502 and 2.511		
Ferraris *et al*. [55]	1.647 and 1.649		2.737, 2.599, 2.633 and 2.720	3.137
Cruciani and Gualtieri [56]	Mean 1.659	2.489, 2.501, 2.520 and 2.524		
Pechar [57]	Mean 1.6512	2.4919	2.6172	
Mazzi *et al*. [58]	1.643, 1.656 and 1.656		in the range from 2.617 to 2.748	
Palmer *et al*. [59]	Mean 1.641, 1.658 and 1.661- natural leuctie Mean 1.640, 1.652 and 1.658 Å for Rb-substitued leucite 1.637, 1.644 and 1.651 Cs 1.668, 1.689 and 1.697 Å for KFeSi2O6			
Hassan *et al*. [60]	1.728, 1.719, 1.612 and 1.623	Mean 2.613		
Simmons and Peacor [61]	Mean 1.697, 1.651, 1.628 and 1.718	in the range from 2.472 to 2.836 with mean 2.58	in the range from 2.48 to 2.88 with mean 2.72	
Tait *et al*. [62]	1.731, 1.723, 1.732, 1.736, 1.728 and 1.734 1.606, 1.603, 1.605, 1.616, 1.615 and 1.616	2.633, 2.632 and 2.627		
Angel *et al*. [63]	in the range from 1.612 to 1.729	in the range from 2.484 to 2.788 Å with mean 2.62		
Dove *et al*. [40]	mean 1.642, 1.649 and 1.658			3.1
White *et al*. [23]	1.75- 1.8			
Geopolymer model of this study	1.8	2.65	2.65	3.1, 3.2 and 3.2

Petkov *et al*. [44] reported a value of 1.6 Å for Si-O distance. In their work, Meral *et al*. and Wyckoff reported the Si-O distance to be 1.62 Å [27, 41]. Yokomori and Idaka studied the crystal structure of nepheline by x-ray diffraction and obtained Si-O lengths around 1.65 Å. They also investigated the Na-O distances and found Na-O distances ranging between 2.502 and 2.511 Å [54]. In their neutron diffraction study of analcime, Ferraris *et al*. obtained Si/Al-O distances of 1.647 and 1.649 Å. They found the O-O distances to be 2.737, 2.599, 2.633 and 2.720 Å and Si/Al-Si/Al distance to be 3.137 Å [55]. Cruciani and Gualtieri reported a mean T-O distance of 1.659 Å for analcime. They obtained Na-O distances of 2.489, 2.501, 2.520 and 2.524 Å [56]. Pechar carried out an x-ray and neutron diffraction analysis on natural monoclinic analcime and obtained a mean T-O distance of 1.6512 Å. He also reported an O-O distance of 2.6172 Å and a mean Na-O distance of 2.4919 Å [57]. Mazzi *et al*. studied the structure of tetragonal leucite and obtained mean T-O distances of 1.643, 1.656 and 1.656 Å for T(1), T(2) and T(3) tetrahedron. They also investigated the O-O distances and obtained results in the range from 2.617 to 2.748 Å [58]. Palmer *et al*. studied the phase transitions in four different leucite phases by high-resolution neutron powder diffraction. They observed mean T-O distances of 1.641, 1.658 and 1.661 Å for natural leucite, 1.640, 1.652 and 1.658 Å for Rb-substitued leucite, 1.637, 1.644 and 1.651 Å for Cs-substitued leucite and 1.668, 1.689 and 1.697 Å for $KFeSi_2O_6$ leucite [59]. Hassan *et al*. studied nepheline structure by single-crystal X-ray diffraction. They observed average Al-O distances of 1.728 and 1.719 Å and Si-O distances of 1.612 and 1.623 Å. They also investigated the Na-O distances and obtained a mean Na-O distance of 2.613 Å [60]. Simmons and Peacor carried out a refinement study to investigate the structure of nepheline from a volcanic environment. They obtained average T-O distances of 1.697, 1.651, 1.628 and 1.718 Å. In addition to the T-O distances, they also investigated the Na-O and O-O distances and found the Na-O distances to be in the range from 2.472 to 2.836 Å with mean 2.58 Å and the O-O distance to be in the range from 2.48 to 2.88 Å and mostly in 2.60 and 2.80 Å range with mean 2.72 Å [61]. Tait *et al*. carried out a refinement study of three nepheline samples. They obtained Al-O distances of 1.731, 1.723, 1.732, 1.736, 1.728 and 1.734 Å. For Si-O pair, they obtained 1.606, 1.603, 1.605, 1.616, 1.615 and 1.616 Å. They also reported the Na-O distance to be 2.633, 2.632 and 2.627 Å [62]. Angel *et al*. studied the crystal structure of nepheline and the structure of the same sample annealed at high temperature using single crystal x-ray diffraction. For T-O distance, they obtained results in

the range from 1.612 to 1.729 Å. They also reported Na-O distances in the range from 2.484 to 2.788 Å with mean 2.62 Å [63]. Dove *et al*. used static lattice energy calculations to study the cubic-tetragonal phase transition in leucite. They observed mean T-O distances of 1.642, 1.649 and 1.658 Å. They reported the T-T distance to be 3.1 Å [40]. White *et al*. investigated the structural characteristics of metakaolin- geopolymer by neutron pair distribution function. They observed Al-O correlation centered around 1.75-1.8 Å for an extensively reacted geopolymer binder [23]. As it is seen from the information summarized above (Table 3.1), interatomic distances obtained from RMC modeling match well with the values reported in the literature.

Partial pair distribution functions, $g_{ij}(r)$, that show the partial contribution of 15 atom pairs to total G(r) are presented in Figures 3.16-3-30:

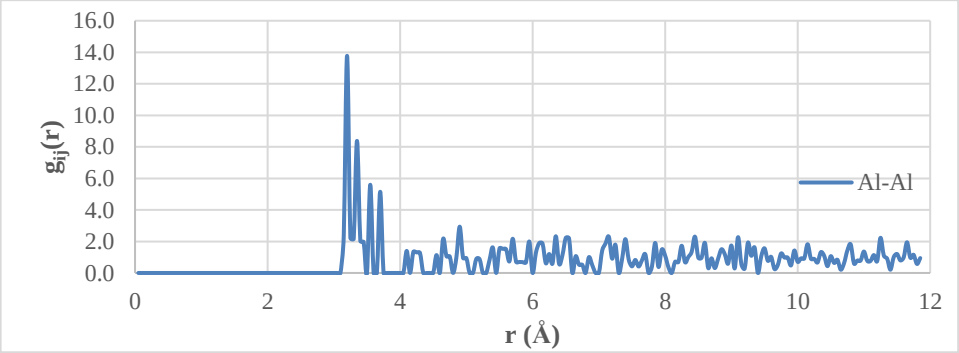

Figure 3.16. Partial pair distribution function results for Al-Al pair in geopolymer model.

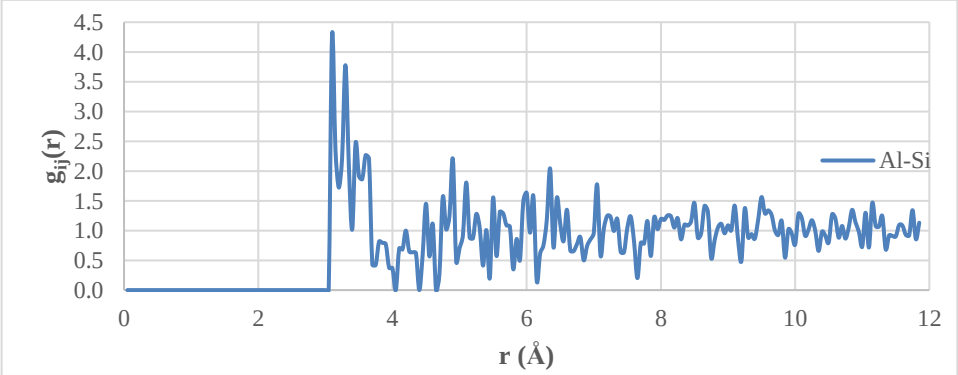

Figure 3.17. Partial pair distribution function results for Al-Si pair in geopolymer model.

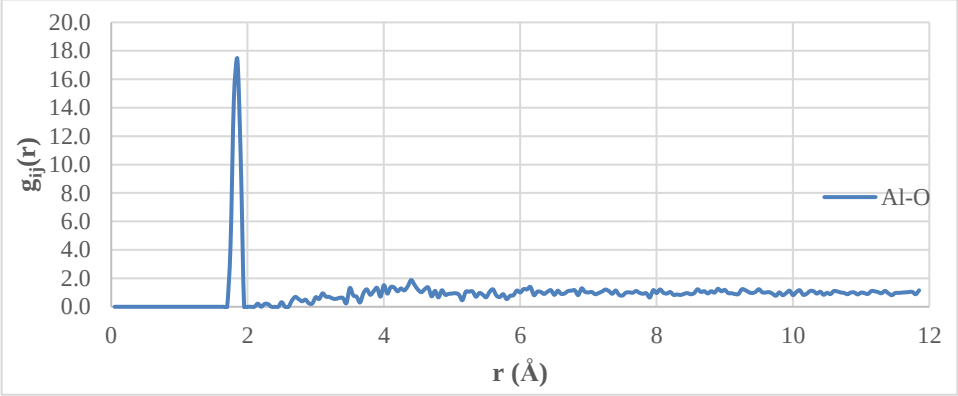

Figure 3.18. Partial pair distribution function results for Al-O pair in geopolymer model.

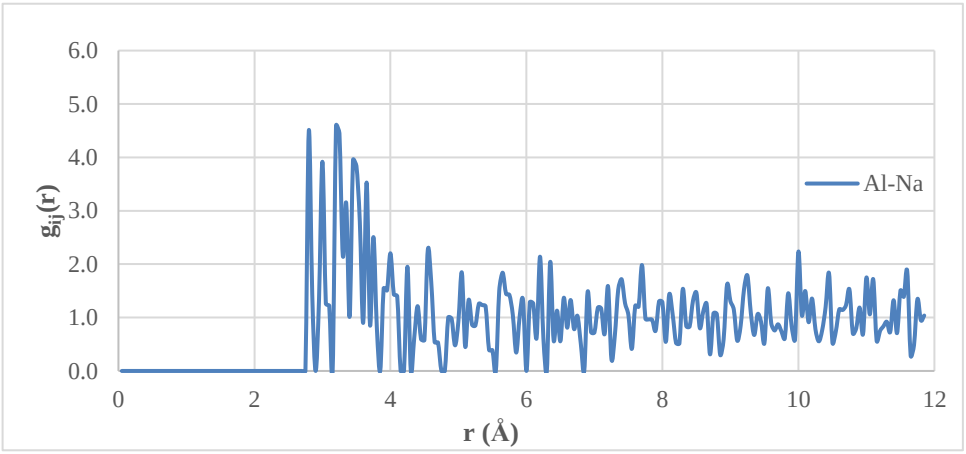

Figure 3.19. Partial pair distribution function results for Al-Na pair in geopolymer model.

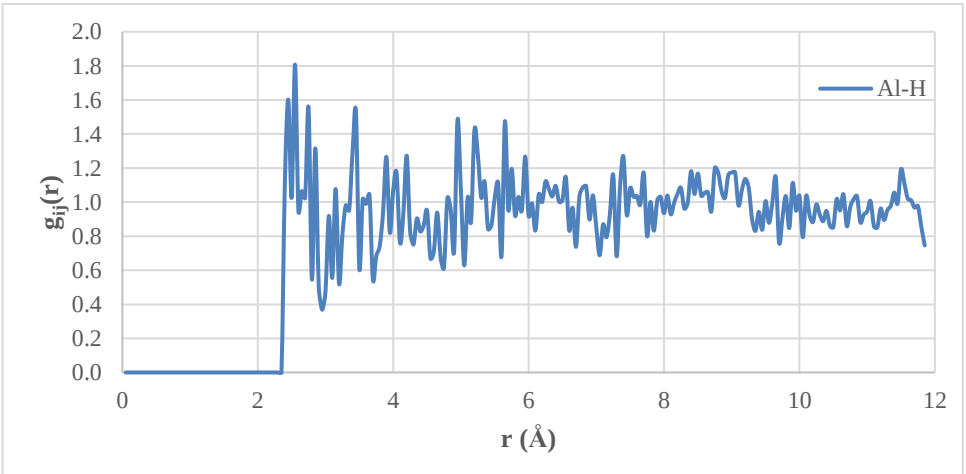

Figure 3.20. Partial pair distribution function results for Al-H pair in geopolymer model.

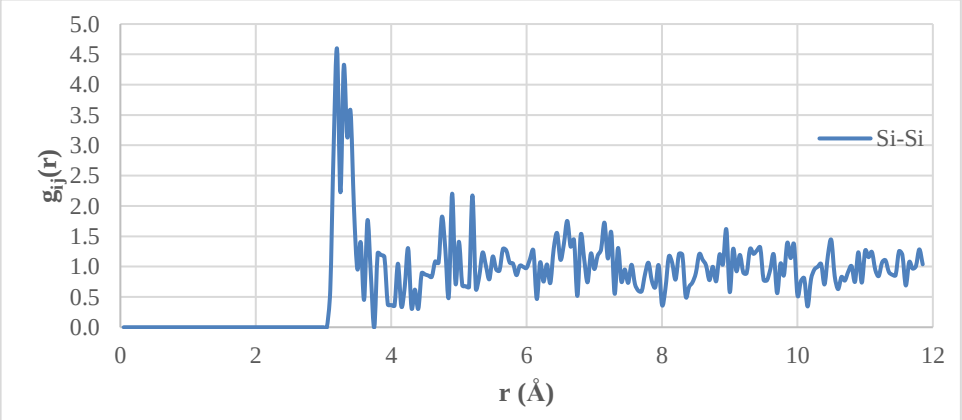

Figure 3.21. Partial pair distribution function results for Si-Si pair in geopolymer model.

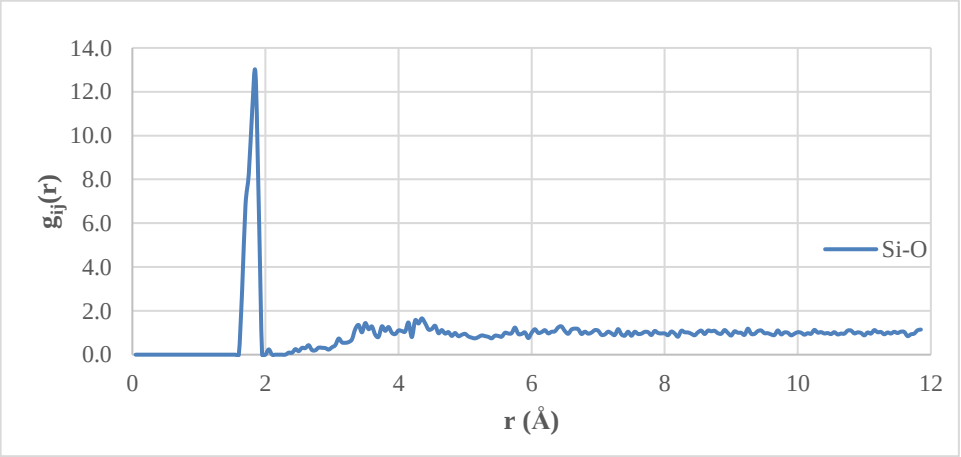

Figure 3.22. Partial pair distribution function results for Si-O pair in geopolymer model.

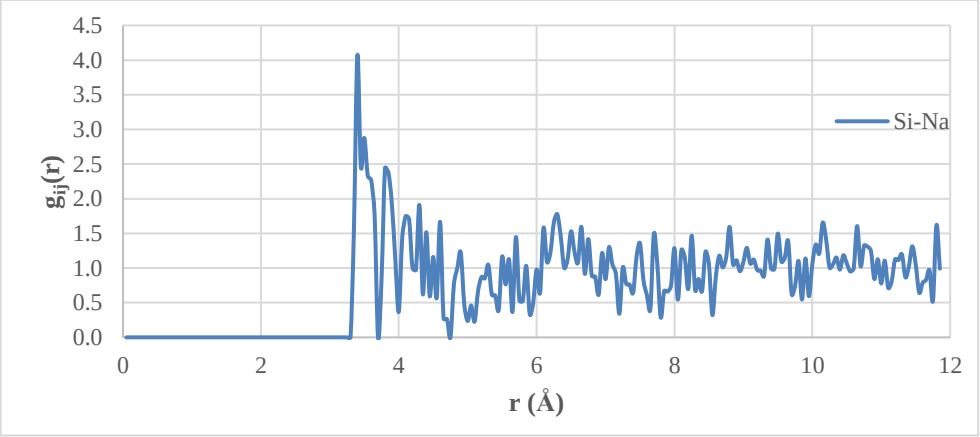

Figure 3.23. Partial pair distribution function results for Si-Na pair in geopolymer model.

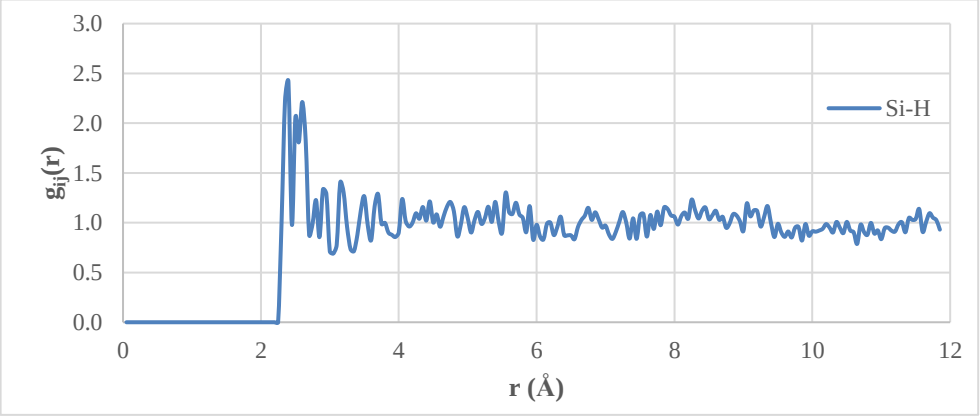

Figure 3.24. Partial pair distribution function results for Si-H pair in geopolymer model.

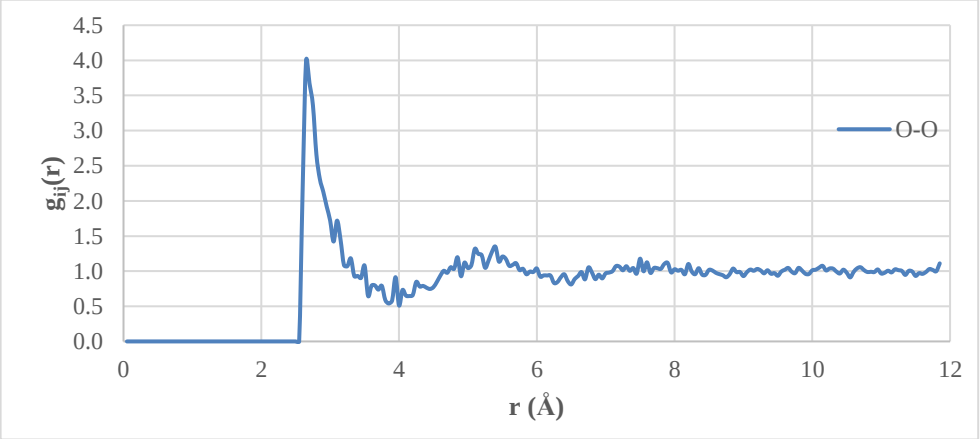

Figure 3.25. Partial pair distribution function results for O-O pair in geopolymer model.

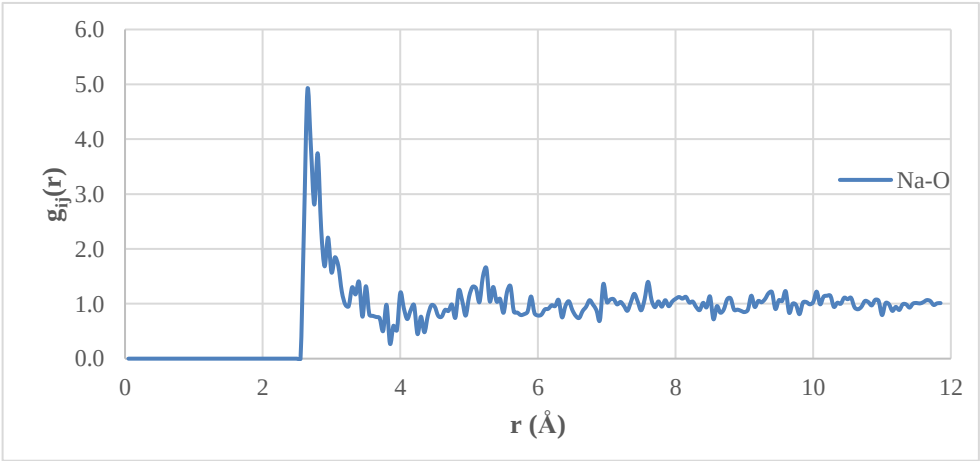

Figure 3.26. Partial pair distribution function results for Na-O pair in geopolymer model.

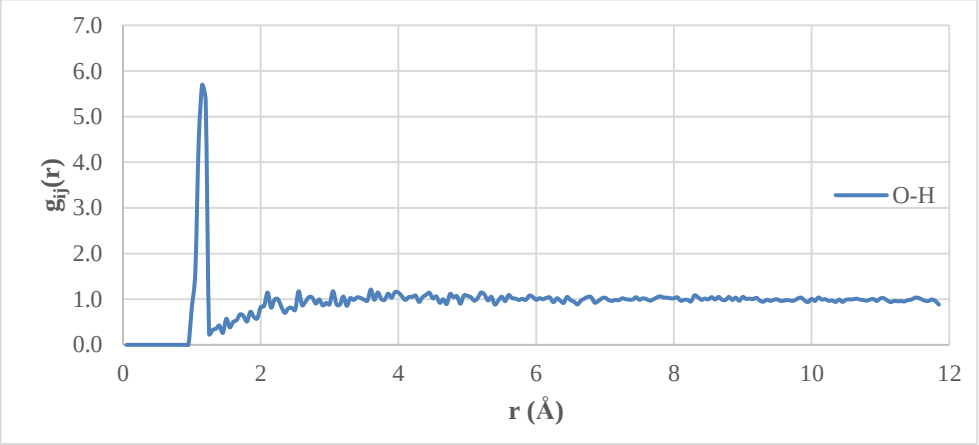

Figure 3.27. Partial pair distribution function results for O-H pair in geopolymer model.

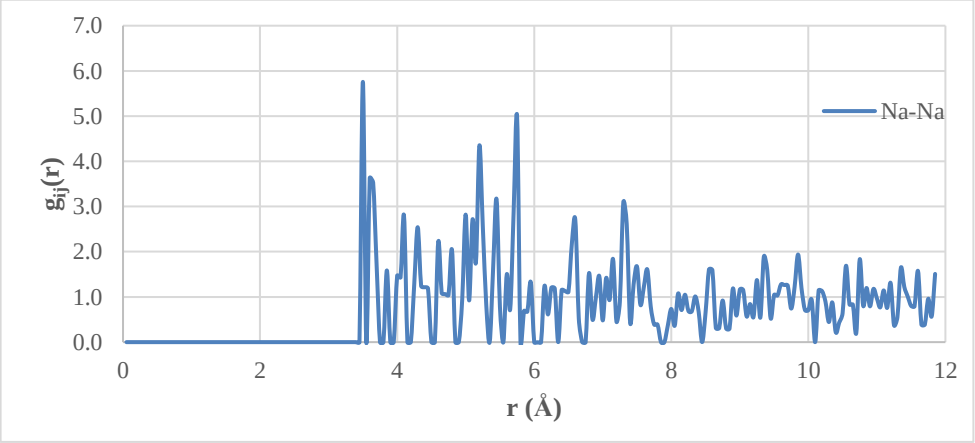

Figure 3.28. Partial pair distribution function results for Na-Na pair in geopolymer model.

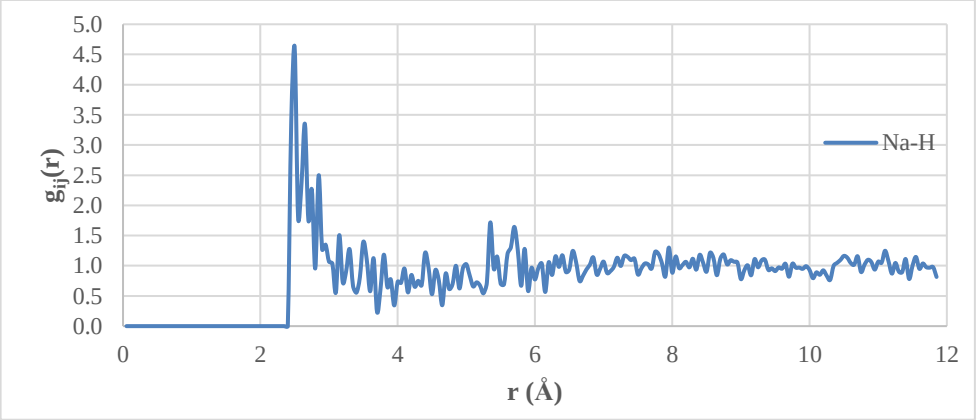

Figure 3.29. Partial pair distribution function results for Na-H pair in geopolymer model.

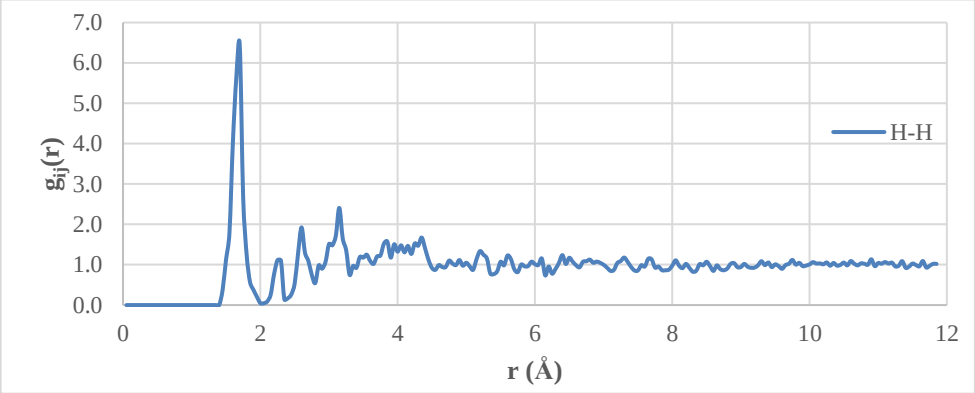

Figure 3.30. Partial pair distribution function data for H-H pair in geopolymer model.

The total G(r) given in Figure 3.15 and the partial distribution functions in Figures 3.16- 3.30 are compared to see the relative contributions of 15 atom pairs to total G(r). Al-O and Si-O correlations seem to be the main contributor to the peak around 1.66 Å, as expected. Furthermore, Na-O pair gives a high intensity peak around 2.65 Å and the O-O pair gives a broad and high intensity peak starting from 2.55 Å. The second peak in Figure 3.15 is centered on 2.65 Å and from the partial g(r) results, it seen that Na-O and O-O correlations are mainly responsible for this peak. The Al-Al and Si-Si pairs seem to be responsible for the peak at 3.1 Å in Figure 3.15. Another peak is present in Figure 3.15, and an investigation of the partial g(r) results given in Figures 3.16- 3.30 reveals that the main contributor to that peak is the Na-Na correlation. In addition to these, there is a peak around 4.2 Å in Figure 3.15 and this peak is attributed to T-O pair in the work by Bell *et al*. [25]. When the partial g(r) of Al-O and Si-O are investigated, it is seen that these two pairs show correlations around 4.2 Å, which agrees with the work by Bell *et al*.

In addition to the above investigations, the coordination environment for Al, Si and Na atoms is also evaluated from the RMC model. The coordination of Al and Si atoms is determined by adding up the number of oxygen atoms falling within a chosen distance of 2.1 Å of that atom, whereas the distance chosen for Na atoms is 3.2 Å. The obtained average coordination numbers for Al, Si and Na are given in Table 3.2.

It is also verified from Table 3.2 that the short-range structure of geopolymer consists of AlO_4 and SiO_4 tetrahedral motifs. Previous NMR studies indicate that Al and Si atoms are tetrahedrally bonded to O atoms [10, 18, 20, 21, 52].

Table 3.2. Average coordination numbers for Na-metakaolin geopolymer model.

Atom	Average Coordination Number
Al	3.90
Si	3.91
Na	6.15

Davidovits describes the products of geopolymerization reaction as cross-linked AlO_4 and SiO_4 tetrahedras [10]. In another study, Davidovits proposed K-geopolymer model based on hydrated leucite. In the proposed model, K^+ cations are located within the alumisilicate matrix and balance negative charge on AlO_4 tetrahedra [64]. Duxson *et al*. states that the Si^{4+} and Al^{3+} cations in the geopolymer structure are tetrahedrally coordinated and linked by oxygen bridges. Alkali ions, Na^+ or K^+, are responsible for balancing the negative charge on the AlO_4^- [65]. Regarding the Na coordination, in their study of crystal structure of analcime, Yokomori and Idaka reported that there are four oxygen atoms and two oxygen atoms from water to give a total of six oxygen atoms around Na atoms [54]. In their study about the crystal structure of natural monoclinic analcime, Pechar reported a Na coordination of 6, consisting of 2 oxygen atoms and 4 oxygen atoms from the water molecules [57]. In his refinement study of nepheline, Dollase reported that the Na atom is coordinated by seven or eight O atoms [66]. In their study of nepheline structure, Hassan *et al*. observed 8 coordination for the Na atom [60]. Tait *et al*. studied the crystal structure of three different nepheline samples and observed that Na atom is 8-coordinated by oxygen atoms [62].

A comparison of the results given in Table 3.2 and the literature results indicate that the obtained coordination results of 3.90 and 3.91 for Al and Si respectively, with geopolymer model agrees well with the literature value of 4 coordination for Al and Si. Furthermore, the average Na coordination for the geopolymer is obtained to be 6.15, which is comparable to the value given for analcime in literature [54, 57]. Analcime ($NaAlSi_2O_6.H_2O$), in terms of chemical composition, is close to the geopolymer system studied here ($NaAlSi_2O_6.5.5H_2O$) except for the water content. It is very interesting to observe that the nearest neighbor environment in terms of bond lengths and coordination environment is very similar for these two stoichiometrically similar systems, analcime and

$NaAlSi_2O_6.5.5H_2O$ geopolymer. On the other hand, a comparison of Na coordination between nepheline and metakaolin- geopolymer reveals that the Na coordination for geopolymer is considerably smaller than 8, which is the Na coordination given for nepheline in literature. In this sense, it can be concluded that the obtained geopolymer model is closer to analcime in terms of Na-O coordination number.

3.2.2.2. Bond Angle Distributions

In this study, the bond angle distributions in geopolymer is obtained based on the RMC model generated and results are compared with the bond angles in minerals namely leucite, nepheline and analcime. T-O-T (Al-O-Al, Si-O-Si, Al-O-Si), O-T-O and Na-O-Na angle distributions are given in Figures 3.31 to 3.37. Table 3.3 presents a comparison of the bond angle values obtained from the RMC model and aforementioned minerals.

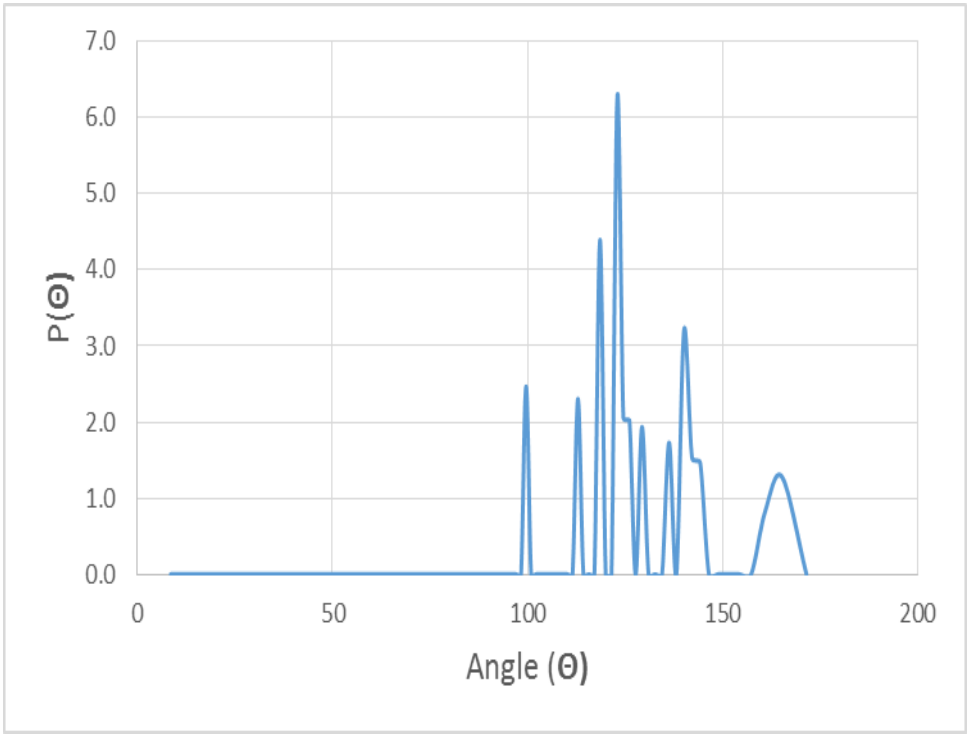

Figure 3.31. Al-O-Al bond angle distribution for metakaolin- geopolymer.

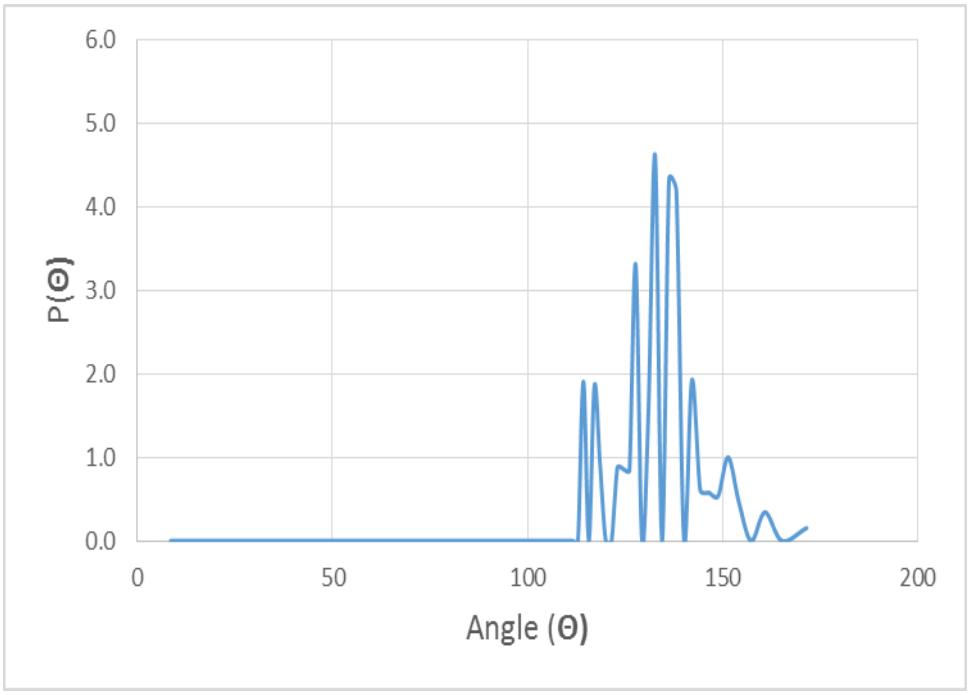

Figure 3.32. Si-O-Si bond angle distribution for metakaolin- geopolymer.

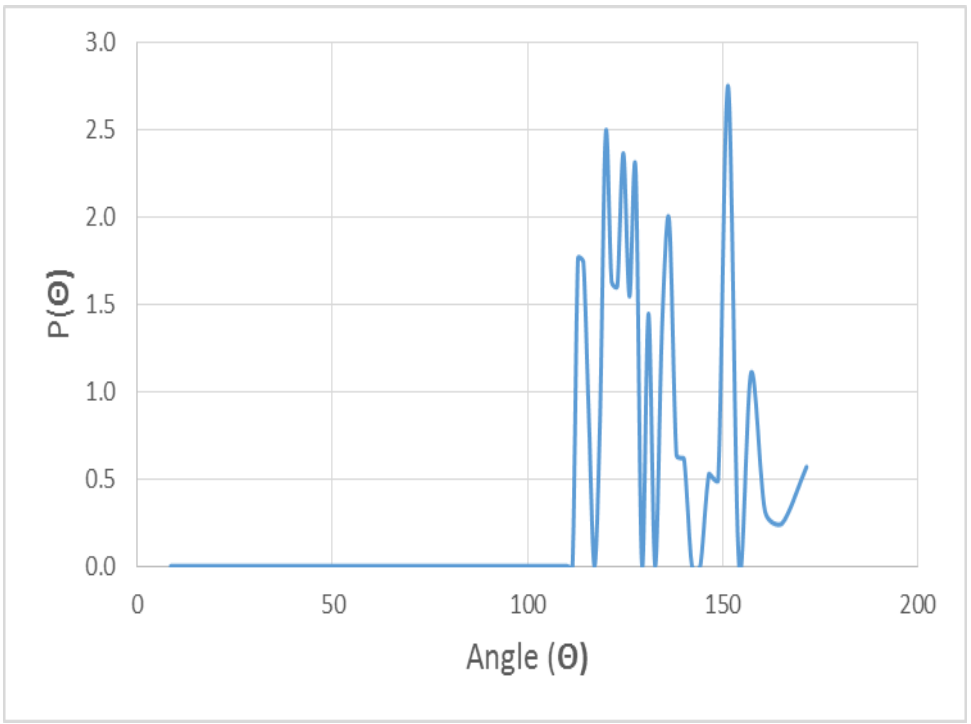

Figure 3.33. Al-O-Si bond angle distribution for metakaolin- geopolymer.

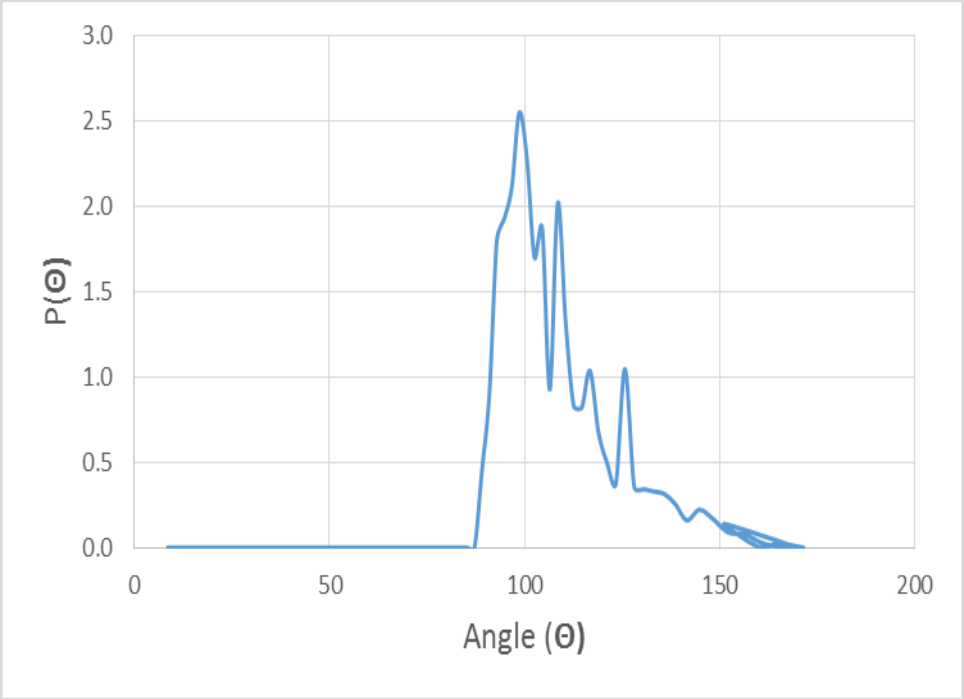

Figure 3.34. O-Si-O bond angle distribution for metakaolin- geopolymer.

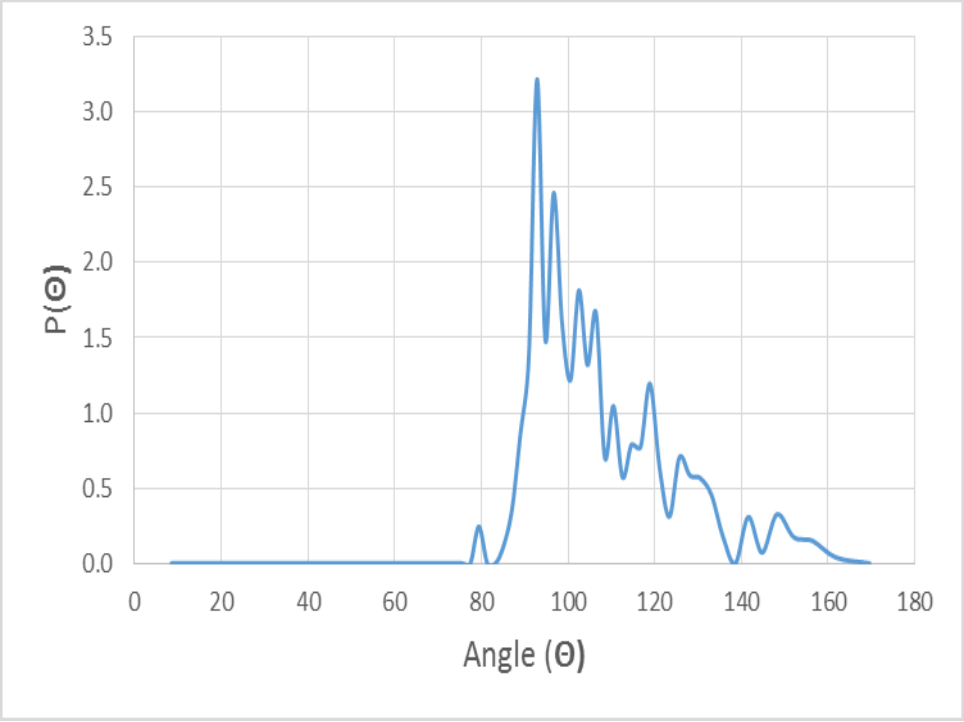

Figure 3.35. O-Al-O bond angle distribution for metakaolin- geopolymer.

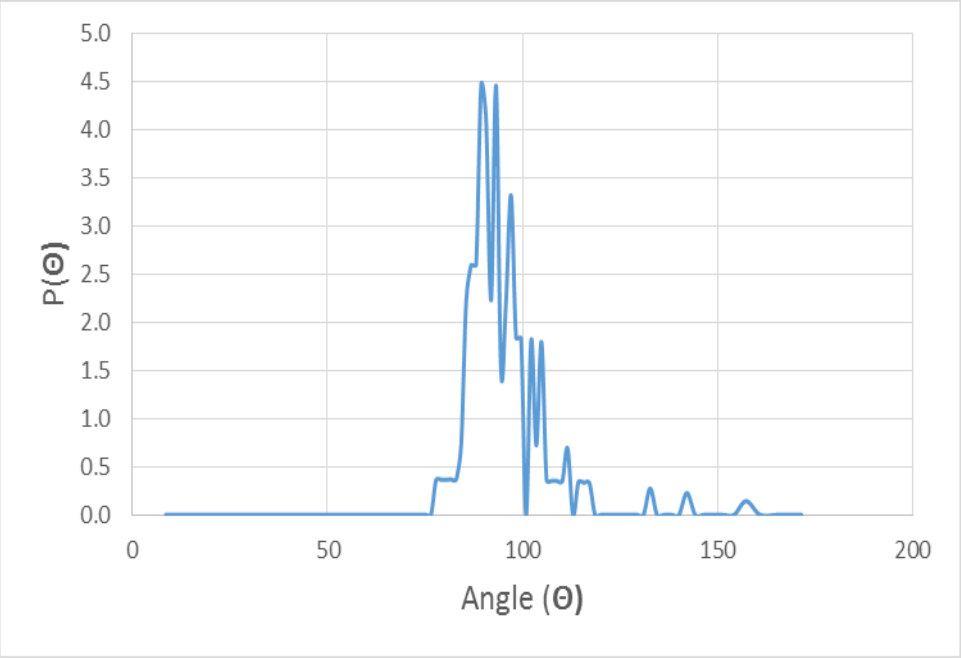

Figure 3.36. H-O-H bond angle distribution for metakaolin- geopolymer.

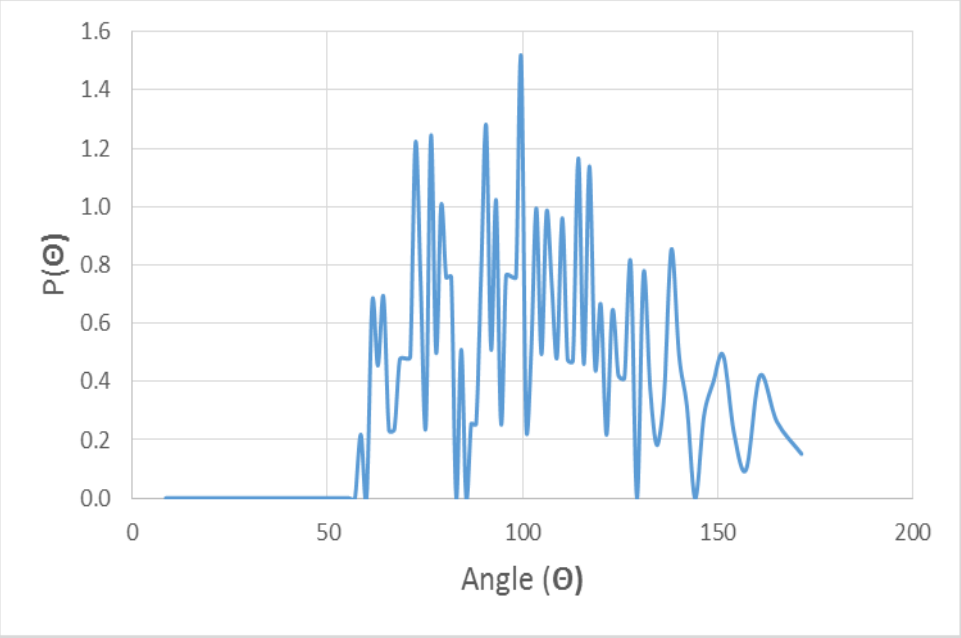

Figure 3.37. Na-O-Na bond angle distribution for metakaolin- geopolymer.

The high intensity peak positions along with the mean angle values for each of the atom triplets given in Figures 3.31-3.37 are presented in Table 3.3. In addition to that, the bond angles for the minerals, which might be considered to be analogs for geopolymer, are given in Table 3.3 and compared with the results of the RMC model.

Table 3.3. Bond angle values for the RMC model of metakaolin-based geopolymer and selected minerals.

	O-T-O Angle (degrees) (O-Al-O or O-Si-O)	**T-O-T Angle (degrees) (Al-O-Al, Si-O-Si or Al-O-Si)**	**Na-O-Na Angle (degrees)**
Analcime	111.3, 104.4, 111.9, 111.9, 106.6, 110.9, 104.3, 112.2,112.2, 110.9, 112.1, 106.2, 111.1, 106.7, 112.0, 112.0, 104.3, 110.9, 112.3, 106.3, 111.1, 110.9, 104.3 and 112.1 (mean 109.5) [54]	144.5 (mean) [54]	120 (mean) [54]
	112.2, 104.2, 111.2, 111.2, 106.0, 112.2 (mean 109.5) [55]	143.5 (mean) [56]	105.15 [57]
	Between 109.43 and 110.46 [57]	144.3 [55]	
Leucite	112.6, 107.4, 111.2, 107.6, 105.7, 112.3, 108.2, 108.1, 111.2, 106.2, 111.5, 111.5 110.5, 109.9, 109.1, 106.7 110.5 and 110.1 (mean 109.46) [58]	Natural leucite 143.6, 153.5, 129.2, 140.6, 130.3 and 129.8 with mean 137.8 Rb substituted leucite 145.5, 156.8, 132.5, 142.1, 134.1 and 132.7 with mean 140.6 Cs substitued leucite 146.7, 152.2, 143.3, 145.1, 138.7 and 137.8 with mean 144.0 $KFeSi_2O_6$ leucite 143.2, 151.5, 126.9, 137.7, 125.2 and 129.7 with mean 135.7 [59]	
	Natural leucite 109.5 (mean) Rb substitued leucite 109.5 (mean) Cs substitued leucite 109.5 (mean) $KFeSi_2O_6$ leucite 109.2 (mean) [59]	144.3, 154.0, 129.7, 140.8, 131.2 and 130.4 138.4 (mean) [58]	
Nepheline	110.0, 93.8, 114.9, 112.3, 112.3 and 112.3 (mean 109.3) [60]	152.5, 138.0, 140.4, 140.4, 141.2 and 141.5 (mean 142.3) [60]	
	111.4, 93.0, 109.7 and 113.7 (mean 107) [61]	156.9, 137.6, 140.5, 140.1, 140.7 and 141.3 (mean 142.9) Mean values for three different samples: 142.9, 143.1, 142.7 [62]	

	115.9, 97.4, 110.7 and 110.7 (mean 108.7) For three different samples values ranging from 97.4 to 115.9 with mean values: 108.7, 108.7, 108.6 [62]	151.0, 137.83, 141.43, 140.75, 141.0 and 141.8 (mean 142.3) [63]	
Geopolymer	93.2 and 106.1 (O-Al-O) mean 114.3 98.3 and 108.8 (O-Si-O) mean 119.5	123.0 (Al-O-Al) mean 132.5 151.3 and 120 (Si-O-Al) mean 135.7 132.7 and 138.1 (Si-O-Si) mean 137.3	99.6 mean 105.9

The bond angle distributions for the obtained geopolymer model along with minerals that are considered as analogs to geopolymer, are given in Table 3.3. In their study, Yokomori and Idaka investigated the crystal structure of trigonal analcime. They obtained values for the O-T-O angle in the range from 104.3 to 112.3 with mean 109.5. They also investigated the T-O-T angles and found them to be ranging in a much narrow range with mean 144.5. In addition to that, they studied the angle between sodium atoms and the water molecules (Na-OW-Na) and found the angle to be 120 [54]. Ferraris *et al*. examined the crystal structure of analcime by neutron diffraction. They found the O-T-O angle to range between 104.2 and 112.2 with mean 109.5. They also found the T-O-T angle to be 144.3 [55]. Cruciani and Gualtieri investigated the changes in the structure of tetragonal analcime after dehydration using temperature-resolved powder diffraction data. They found the average T-O-T angle to be 143.5 at 298 K [56]. Pechar performed an x-ray and neutron diffraction analysis on natural monoclinic analcime. He found the tetrahedral angle to be deformed between 109.43 and 110.46. He also investigated the Na-O-Na angles and found the mean angle to be 105.15 [57].

In their work, Mazzi *et al*. studied the structure of tetragonal leucite. They observed O-T-O angles ranging from 105.7 to 112.6 with mean 109.46. They also investigated the T-O-T angles and determined the values to range between 129.7 and 154.0 and the mean to be 138.4 [58]. Palmer *et al*. used high- resolution neutron powder diffraction to study phase transitions in $KAlSi_2O_6$, $RbAl_2Si_6$, $CsAlSi_2O_6$ and $KFeSi_2O_6$. They investigated the O-T-O angles and found the mean angle to be 109.5 for natural, Rb-exchanged and Cs-exchanged leucite and 109.2 for $KFeSi_2O_6$. They also studied the T-O-T angles and found the angles to

be 137.8 for natural leucite, 140.6 for Rb-exchanged leucite, 144.0 for Cs-substitued leucite and 135.7 for $KFeSi_2O_6$ [59].

In their work, Hassan *et al*. studied the nepheline structure by x-ray diffraction. They obtained O-T-O angles ranging from 93.8 to 114.9 with a mean value of 109.3. They also investigated T-O-T angles and obtained a mean angle of 142.3 [60]. Simmons and Peacor refined the structure of nepheline from a volcanic environment. They obtained O-T-O angle to be between 93 and 113.7 with mean 107 [61]. Tait *et al*. refined the structures of three nepheline samples from Russia, Canada and Italy. They observed small differences in the O-T-O angles of three samples with mean values of 108.7, 108.7 and 108.6. Similarly, small differences were present for the mean T-O-T angles. They found the mean T-O-T angles to be 142.9, 143.1 and 142.7 for the three samples they worked with. Even though the average for all three cases was around 143, they observed a T-O-T angle around 156 for all three samples [62]. Angel *et al*. studied the crystal structures of nepheline and nepheline annealed at high temperature using single-crystal X-ray diffraction. They observed T-O-T angles ranging from 137.83 to 151.0 and the average T-O-T angle of 142.3 [63].

The bond angle distribution for the obtained geopolymer model gives high intensity peaks at 93.2 and 104.5 for O-Al-O angle, and 98.3 and 108.8 for O-Si-O angles. These results are smaller than 109.5, which is the expected result for a tetrahedral unit. An investigation of the bond angles given in Table 3.2 reveals that the mean O-T-O angles are around 109.5 for all the minerals. On the other hand, when individual angles, instead of the mean values, are investigated, it is seen that the results given for nepheline cover a large area with values ranging between 93.8 and 114.9 in the work by Hassan *et al*.[60]. This result, along with the other results given for nepheline in Table 3.2, indicates a distortion of the O-T-O angle. In fact, Simmons and Peacor argues that such distortion is characteristic of other refined nepheline structures [61]. Dollase and Hassan *et al*. explains that the unusual bond angles are observed because of the displaced oxygen atom, which results from the adjustment of the oxygen atom to form reasonable Na-O bonds [60, 66]. In this sense, the distortion in O-T-O bond angles in our model can be possibly explained with the same reasoning.

The average of the mean angles for Al-O-Al, Si-O-Si and Al-O-Si for the geopolymer model is 135.2. When the average T-O-T angle is compared with the mean T-O-T angles of analcime, it is seen that the mean T-O-T angle is smaller than the T-O-T angle given by Yokomori, Ferraris and Cruciani [54-56]. A similar conclusion can be drawn if the average T-O-T angles of nepheline are compared with that of the geopolymer. On the other hand, the situation is different when the average T-O-T angles for leucite and geopolymer are compared. In Mazzi *et al.*'s work, the average T-O-T bond angle is found to be 138.4 [58]. Similarly, Palmer *et al*. obtained average T-O-T angles of 137.8 and 135.7 for natural leucite and $KFeSi_2O_6$ leucite respectively [59]. These results are comparable to the average T-O-T angle of 135.2, which is obtained with the geopolymer model. Individual angles from previous studies, instead of the mean values, are also compared with the values of the peak positions in the geopolymer bond angle distribution. Palmer *et al*. [59] gives different T-O-T bond angles, ranging between 129.2 and 153.5 and some intermediate values around 140 for natural leucite, which are comparable to the results of 151.3, 138.1 and 123 that are obtained at the high intensity positions of bond angle distribution results. Although comparable, the results obtained for the geopolymer are slightly lower than the results for leucite. In their work, Tait *et al*. observed that shorter T-O distances resulted in larger T-O-T angles [62]. The T-O bond distances in the geopolymer model are slightly higher than the expected results (1.8 vs. 1.7 Å). Considering the observations of Tait *et al*., the slightly lower bond angles can be explained with the larger T-O distances obtained for the geopolymer.

Two different Na-O-Na angles are given in Table 3.3. The Na-O-Na angle given in the work by Yokomori and Idaka [54] is for the sodium atoms and the oxygen atoms of the water molecules. On the other hand, Pechar gives a mean Na-O-Na angle of 105.15 [57]. A comparison of the Na-O-Na bond angle for analcime and the obtained geopolymer model reveals that the Na-O-Na bond angle obtained for the geopolymer is comparable to the results given in Pechar's work with mean values of 105.15 and 105.90.

3.2.2.3. Intermediate-Range Order (IRO)

Information regarding intermediate-range order in geopolymer systems has been lacking in the literature to date. This is partly due to the difficulties arising from the fact that

these are disordered and multicomponent complex systems. In this study, RMC modeling is employed to generate a 3D geopolymer structure that meets the short-range order constraints outlined in the literature and is in agreement with the experimental data collected for this system. This model is then also used to extract information on IRO in this system. For this purpose, a ring size distribution analysis is carried out using ISAACS software [67]. King's algorithm, in which the definition of a ring is made as the shortest path to a given node from one of the neighbor atoms, is used in the ring analysis [68]. Radius of the first coordination sphere for each chemical species and first minimum of the total RDF are given as inputs to the software. 3.1, 1.8 and 2.6 A are taken as the radius of the first coordination sphere for T-T (T: Al or Si), T-O and O-O pairs, respectively, and the first minimum of the total RDF is given as 2.1 to the software. The ring size distribution obtained for the geopolymer system is given in Figure 3.38. The results based on this analysis indicated that 7 and 8 membered rings are dominant in the geopolymer structure with somewhat high amount of 6 membered rings. These nano-scale structural motives are thought to be responsible for the IRO in this system. 2-, 3-, 4-, and 5- membered rings seem to be present as minority compared to larger rings. The ring size distributions obtained in this system are compared with the ring sizes reported for minerals, namely leucite, analcime and nepheline.

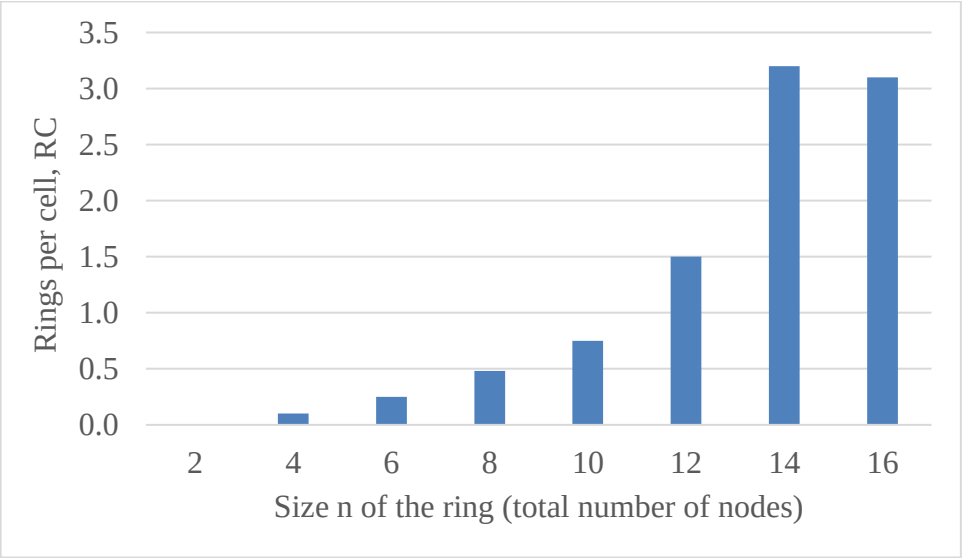

Figure 3.38. Ring size distribution for metakaolin-masked geopolymer. n represents the total number of nodes.

There are various studies in the literature that deal with the ring sizes present in the structure of these minerals that can be used as structural analogs to geopolymers. For instance, Ferraris *et al*. carried out a neutron diffraction study on the crystal structure of analcime, where an aluminosilicate framework consisting of rings of six and four tetrahedral formed by SiO_4 and AlO_4 tetrahedra is reported [55]. In their in situ synchrotron powder diffraction study on dehydration dynamics of analcime, Cruciani and Gualtieri reported four, six and eight membered tetrahedral rings [56]. Palmer *et al*., based on their high- resolution neutron powder diffraction study on phase transitions in three different leucite phases, stated that leucite structure is made up of a framework consisting of fourfold, sixfold and eightfold rings of $(Al,Si)O_4$ tetrahedra [59]. In his work, Zoltai reported 4-6 and 8 fold repeat-units and loops of tetrahedra for leucite [69]. In their work, Papike and Cameron pointed out that the structure of nepheline is dominated by six-membered rings of TO_4 tetrahedra [70]. Hassan *et al*. reported six- membered hexagonal rings in the structure of nepheline [60]. Similarly, Tait *et al*., Angel *et al*. and Zoltai stated that the nepheline structure comprises 6 membered rings [62, 63, 69]. Based on these studies, 4-, 6-, and 8 membered rings are reported to exist in analcime and leucite structures whereas nepheline structure seems to involve only 6-membered rings. The ring size distribution presented in Figure 3.38 shows that a much wider variety of ring sizes exists in geopolymer structure compared to these minerals. This is not suprising as geopolymer is a highly disordered system. IRO structure in this system can be thought to be somewhat closer to analcime and leucite systems.

The Na atoms in the geopolymer structure are known to act as charge balancing cations. By using the RMC model of this study, Na-O coordination is found to be 6.15 (taking a cut off distance of 3.2 Å). The ring size distribution analysis in the RMC geopolymer model yielded rings consisting of mostly 7 and 8 membered rings along with some 6 membered rings. When the average Na-O coordination number and the ring analysis results are taken into consideration, it can be argued that the Na atoms are located in the large rings present in the structure and these two results complement each other.

4. CONCLUSIONS AND RECOMMENDATIONS

In this study, a geopolymer with an approximate composition of $NaAlSi_2O_6.5.5H_2O$ is synthesized using metakaolin powder and a mixture of sodium hydroxide and sodium silicate solution as the activating solution. Metakaolin is obtained by calcination of kaolinite mineral at 700°C for an hour. High-energy x-ray diffraction measurements are carried out for kaolinite, metakaolin and metakaolin based geopolymer. Reverse Monte Carlo (RMC) modeling technique is used to generate three-dimensional structural models of metakaolin and geopolymer systems based on the experimental diffraction data.

Comparison of experimental total structure factors and radial distribution functions of kaolinite and metakaolin, showed that high temperature dehydroxylation process results in transformation of crystalline kaolinite that consists of ordered Si and Al layers into a predominantly disordered structure. At short-range scale, the main effect of calcination at 700 °C is the change in the Al coordination in the system from octahedral to mainly tetrahedral as Si atoms are always tetrahedrally coordinated to O atoms.

RMC model of metakaolin clearly indicates that Al and Si layers present in kaolinite structure are preserved after dehydroxylation. However, Al and Si layers seem quite distorted and buckled, which is in agreement with the previous studies regarding dehydroxylation of kaolinite. The interatomic distance between Al and Si layers in metakaolin structure is found to be 3.1 Å based on the Al-Si partial pair distribution function results.

RMC model of geopolymer consists of crosslinked AlO_4 and SiO_4 tetrahedral units where Na atoms seem to be randomly distributed throughout the structure. The bond angle distributions for the geopolymer model are obtained and are found to be comparable to mainly mineral leucite. A ring size distribution analysis is performed on this model to investigate intermediate-range order in the system. The results indicate that the geopolymer structure predominantly involves seven and eight membered rings consisting of TO_4 (T: Si, Al) units together with considerable amount of six-membered rings. Geopolymer structure

seems to contain a wider variety of ring sizes compared to its crystalline structural analogs namely, leucite, anacime and nepheline.

In this study, it is found that the intermediate-range order in metakaolin-based geopolymer system consists predominantly of 6- to 8-membered rings. It would be interesting to carry out small angle x-ray scattering (SAXS) experiments that would complement the findings of the current study. SAXS will be extremely valuable since it will provide information regarding possible inhomogeneities in the system that extend to nanometer length-scales which could then be linked to the presence of larger rings proposed by this study.

REFERENCES

1. Li, C., X. Gong, S. Cui, Z. Wang, Y. Zheng, B. Chi, "CO_2 emissions due to cement manufacture", *Mater. Sci. Forum*, Vol. 685, pp. 181- 187, 2011.

2. Huntzinger, D.N., T.D. Eatmon, "A life-cycle assessment of cement manufactoring: comparing traditional process with alternative technologies", *Journal of Cleaner Production*, Vol. 17, pp. 668-675, 2009.

3. Turner, L.K., F.G. Collins, "Carbon dioxide equivalent (CO_2-e) emissions: a comparison between geopolymer and OPC cement concrete", *Construction and Building Materials*, Vol. 43, pp. 125-130, 2013.

4. White, C.E., J.L. Provis, B. Bloomer, J.L. Henson, K. Page, "In situ X-ray pair distribution function analysis of geopolymer gel nanostructure formation kinetics", *Physical Chemistry Chemical Physics*, Vol. 15, pp. 8573-8582, 2013.

5. van Deventer, J.S.J., J.L. Provis, P. Duxson, D.G. Brice, "Chemical research and climate change as drivers in the commercial adoption of alkali activated materials ", *Waste and Biomass Valorization*, Vol. 1, pp. 145-155, 2010.

6. Davidovits, J., *Geopolymer Chemistry and Applications*, Instute Geopolymer, Morrisville, 2008.

7. Temuujin, J., W. Rickard, A. van Riessen, "Characterization of various fly ashes for preparation of geopolymers with advanced applications", *Advanced Powder Technology*, Vol. 24, pp. 495-498, 2013.

8. Temuujin, J., A. Minjigmaa, W. Rickard, M. Lee, I. Williams, A. van Riessen, "Fly ash based geopolymer thin coatings on metal substrates and its thermal evaluation", *Journal of Hazardous Materials*, Vol. 180, pp. 748-752, 2010.

9. Bakharev, T., "Resistance of geopolymer materials to acid attack", *Cement and Concrete Research*, Vol. 35, pp. 658-670, 2005.

10. Davidovits, J., "Geopolymers", *Journal of Thermal Analysis*, Vol. 37, pp. 1633-1656, 1991.

11. Palomo, A., F.P. Glasser, "Chemically- bonded cementitious materials based on metakaolin", *British Ceramic. Transactions and Journal*, Vol. 91, pp. 107-112, 1992.

12. Glukhovsky, V.D., G.S. Rostovskaja, G.V. Rumyna, "High strength slag-alkaline cements ", *Proceedings of the 7th International Congress on the Chemistry of Cement*, Vol. 3, pp. 164-168, 1980.

13. van Jaarsveld, J.G.S., J.S.J. van Deventer, G.C. Lukey, "The effect of composition and temperature on the properties of fly-ash and kaolinite- based geopolymers", *Chemical Engineering Journal*, Vol. 89, pp. 63-73, 2002.

14. Duxson, P.J.L.P., G.C. Lukey, S.W. Mallicot, W.M. Kriven, J.S.J. van Deventer, "Understanding the relationship between geopolymer compositon, microstructure and mechanical properties", *Colloids and Surfaces A: Physicochemical and Engineering Aspects*, Vol. 269, pp. 47-58, 2005.

15. Panias, D., I. P. Giannopoulou, T. Perraki, , "Effect of synthesis parameters on the mechanical properties of fly ash- based geopolymers", *Colloids and Surfaces A: Physicochemical and Engineering Aspects*, Vol. 301, pp. 246-254, 2007.

16. Xu, H., J.S.J. van Deventer, "Geopolymerisation of multiple minerals", *Minerals Engineering*, Vol. 15, pp. 1131-1139, 2002.

17. Engelhardt, G., D. Michel, *High- Resolution Solid State NMR of Silicates and Zeolites*, John Wiley & Sons Ltd, Chichester, 1987.

18. Singh, P.S., T. Bastow, M. Trigg, "Structural Studies of Geopolymers by 29Si and 27Al MAS-NMR", *Journal of Materials Science*, Vol. 40, pp. 3951-3961, 2005.

19. Davidovits, J., Orlinski, J., "Geopolymer Chemistry and Properties", *First European conference on soft mineralurgy* Universite De Technologie De Compeigne, 1988.

20. Barbosa, V., K. Mackenzie, C. Thaumaturgo, "Synthesis and characterisation of materials based on inorganic polymers of alumina and silica: sodium polysialate polymers", *International Journal of Inorganic Materials*, Vol. 2, pp. 309-317, 2000.

21. Duxson, P.J.L.P., G.C. Lukey, F. Separovic, J.S.J. van Deventer, "29Si NMR study of structural ordering in aluminosilicate geopolymer gels", *Langmuir*, Vol. 21, pp. 3028-3036, 2005.

22. Egami, T., Billinge, S.J.L., *Underneath the Bragg peaks: structural analysis of complex materials*, Elsevier Ltd., Amsterdam, 2002.

23. White, C.E., J.L. Provis, T. Proffen, J.S.J. van Deventer, "The effects of temperature on the local structure of metakaolin-based geopolymer binder: a neutron pair distribution function investigation", *J. Am. Ceram. Soc.*, Vol. 93, pp. 3486-3492, 2010.

24. White, C.E., J.L. Provis, A. Llobet, T. Proffen, J.S.J. van Deventer, "Evolution of local structure in geopolymer gels: an in situ neutron pair distribution function analysis", *J. Am. Ceram. Soc.*, Vol. 94, pp. 3532-3539, 2011.

25. Bell, J.L., P. Sarin, P.E. Driemeyer, R.P. Haggerty, P.J. Chupas, W.M. Kriven, "X-Ray pair distribution function analysis of a metakaolin-based, $KAlSi_2O_6$ $5.5H_2O$ inorganic polymer (geopolymer)", *Journal of Materials Chemistry*, Vol. 18, pp. 5974-5981, 2008.

26. Bell, J.L., P. Sarin, J.L. Provis, R.P. Haggerty, P.E. Driemeyer, P.J. Chupas, J.S.J.van Deventer, W.M. Kriven, "Atomic structure of a cesium aluminosilicate geopolymer: A pair distribution function study", *Chemistry of Materials*, Vol. 20, pp. 4768-4776, 2008.

27. Meral, C., C.J. Benmore, P.J.M. Monteiro, "The study of disorder and nanocrystallinity in C–S–H, supplementary cementitious materials and geopolymers using pair distribution function analysis", *Cement & Concrete Research*, Vol. 41, pp. 696-710, 2011.

28. Mcgreevy, R.L., L. Pusztai, "Reverse Monte Carlo simulation: a new technnique for the determination of disoredered structures", *Molecular Simulation*, Vol. 1, pp. 359-367, 1988.

29. Ozer, I., S. Soyer-Uzun, "Relations between the structural characteristics and compressive strenght in metakaolin based geopolymers with different molar Si/Al ratios", *Ceramics International*, Vol. 41, pp. 10192-10198, 2015.

30. Williams, R.P., A. van Riessen, "Development of alkali activated borosilicate inorganic geopolymers", *J.Eur. Ceram. Soc.*, Vol. 31, pp. 1513-1516, 2011.

31. Duxson, P., S.W. Mallicoat, G.C. Lukey, W.M. Kriven, J.S.J. van Deventer, "The effect of alkali and Si/Al ratio on the development of mechanical properties of metakaolin based geopolymers", *Colloids Surf. A*, Vol. 292, pp. 8-20, 2007.

32. Rowles, M., B. O'Connor, "Chemical optimisation of the compressive strenght of aluminasilicate geopolymers synthesised by sodium silicate activation of metakaolinite", *J. Mater. Chem.*, Vol. 13, pp. 1161-1165, 2003.

33. Skinner, L.B., C.J. Benmore, J.B. Parise, "Area detector corrections for high quality synchrotron x-ray structure factor measurements", *Nuc. Instr: Methods A*, Vol. 662, pp. 61-70, 2012.

34. Benmore, C.J., "A review of high- energy x-ray diffraction from glasses and liquids", *ISRN Materials Science*, Vol. 2012, 2012.

35. Metropolis, N., A.W. Rosenbluth, M.N., Rosenbluth, A. H. Teller, E. Teller, "Equation of state calculations by fast computing machines", *J. Chem. Phys.*, Vol. 21, pp. 1087-1092, 1953.

36. McGreevy, R.L., "Reverse Monte Carlo modeling", *Journal of Physics: Condensed Matter*, Vol. 13, pp. 877-913, 2001.

37. Dove, M.T., M.G. Tucker, S.A. Wells, D.A. Keen, "Reverse Monte Carlo methods", *EMU Notes in Mineralogy*, Vol. 4, pp. 59-82, 2002.

38. White, C.E., J.L. Provis, T. Proffen, D.P. Riley, J.S.J. van Deventer, "Combining density functional theory (DFT) and pair distribution function (PDF) analysis to solve the structure of metastable materials: the case of metakaolin," *Physical Chemistry Chemical Physics*, Vol. 12, pp. 3239-3245, 2010.

39. Al-Akhras, N., "Durability of metakaolin concrete to sulfate attack", *Cement & Concrete Research*, Vol. 36, pp. 1727-1734, 2006.

40. Dove, M.T., T. Cool, D.C. Palmer, A. Putnis, E.K.H. Salje, B. Winkler, "On the role of Al-Si ordering in the cubic- tetragonal phase transition of leucite", *American Mineralogist*, Vol. 78, pp. 486-492, 1993.

41. Wyckoff, R.W.G., *Crystal structures*, Interscience Publishers, New York, 1968.

42. Sakkas, K., S. Kapelari, D. Panias, P. Nomikos, A. Sofianos, "Fire resistant K-based metakaolin geopolymer for passive fire protection of concrete tunnel linings", *Open Access Library Journal*, Vol. 1, pp. 1-9, 2014.

43. Arı, M.U., M.G. Ahunbay, M. Yurtsever, A. Erdem- Senatalar, "Molecular dynamics simulation of water diffusion in MFI-type zeolites", *Journal of Physical Chemistry B*, Vol. 113, pp. 8073-8079, 2009.

44. Petkov, V., S.J.L. Billinge, S.D. Shastri, B. Himmel, "Polyhedral units and network connectivity in calcium aluminosilicate glasses from high-energy x-ray diffraction", *Physical Review Letters*, Vol. 85, pp. 3436-3439, 2000.

45. Toukan, K., A. Rahman, "Molecular dynamics study of atomic motions in water ", *Physical Review B*, Vol. 31, pp. 2643-2648, 1985.

46. Klinowski, J., P.J. Barrie, *Recent advances in zeolite science*, Elsevier, Cambridge, 1990.

47. McKeown, D.A., G.A. Waychunas, G.E. Brown Jr, "Exafs and xanes study of the local coordination environment of sodium in a series of silica- rich glasses and selected minerals within the $Na_2OAl_2O_3SiO_2$ system", *Journal of Non-Crystalline Solids*, Vol. 74, pp. 325-348, 1985.

48. Greaves, G.N., Y. Vaills, S. Sen, R. Winter, "Density fluctuations, phase seperation and microsegregation in silicate glasses ", *Journal of Optoelectronics and Advanced Materials*, Vol. 2, pp. 299-316, 2000.

49. Sperinck, S., P. Raiteri, N. Marks, K. Wright, "Dehydroxylation of kaolinite to metakaolin - a molecular dynamics study", *Journal of Materials Chemistry*, Vol. 21 pp. 2118-2125, 2011.

50. White, C.E., J.L. Provis, T. Proffen, D.P. Riley, J.S.J. van Deventer, "Density functional modeling of the local structure of kaolinite subjected to thermal dehydroxylation", *J. Phys. Chem. A*, Vol. 114, pp. 4988-4996, 2010.

51. Dennington, R., T. Keith, J. Milliam, *GaussView, Version 3*, 2009, Semichem Inc. Shawnee Mission KS.

52. Davidovits, J., J. Orlinski, "Geopolymer chemistry and properties", in G. Institute, *First European Conference on Soft Mineralurgy*, Universite De Technologie De Compeigne, 1988

53. Cusack, N.E., *The physics of structurally disordered matter*, A. Hilger, Philadelphia, 1987.

54. Yokomori, Y., S. Idaka, "The crystal structure of analcime", *Microporous and Mesoporous Materials*, Vol. 21, pp. 365-370, 1998.

55. Ferraris, G., D.W. Jones, J. Yerkess, "A neutron-diffraction study of the crystal structure of analcime, NaAISi206.H20", *Zeitschrift für Kristallographie*, Vol. 135, pp. 240-252, 1972.

56. Cruciani, G., A. Gualtieri, "Dehydration dynamics of analcime by in situ synchrotron powder diffraction", *American Mineralogist*, Vol. 84, pp. 112-119, 1999.

57. Pechar, F., "The crystal structure of natural monoclinic analcime ($NaAISi_20_6$. H_20)", *Zeitschrift fur Kristallographie*, Vol. 184, pp. 63-69, 1988.

58. Mazzi, F., E. Galli, G. Gottardi, "The crystal structure of tetragonal leucite", *American Mineralogist*, Vol. 61, pp. 108-115, 1976.

59. Palmer, D.C., M.T. Dove, R.I. Ibberson, B.M. Powell, "Structural behaviour, crystal chemistry, and phase transitions in substitued leucite: High- resolution neutrın powder diffraction studies", *American Mineralogist*, Vol. 82, pp. 16-29, 1997.

60. Hassan, I., S.M. Antao, A.A.M. Hersi, "Single- crystal XRD, TEM, and thermal studies of the satellite reflections in nepheline", *The Canadian Mineralogist*, Vol. 41, pp. 759-783, 2003.

61. Simmons, W.B., D.R. Peacor, "Refinement of the crystal structure of a volcanic nepheline", *American Mineralogist*, Vol. 57, pp. 1711-1719, 1972.

62. Tait, K.T., E. Sokolova, F.C. Hawthorne, "The crystal chemistry of nepheline", *The Canadian Mineralogist*, Vol. 41, pp. 61-70, 2003.

63. Angel, R.J., G.D. Gatta, T.B. Ballaran, M.A. Carpenter, "The mechanism of coupling in the modulated structure of nepheline", *The Canadian Mineralogist*, Vol. 46, pp. 1465-1476, 2008.

64. Davidovits, J., "Geopolymere", *2nd International Conference on Geopolymers*, Saint-Quentin, France, 1999

65. Duxson, P., A. Fernandez-Jimenez, J.L. Provis, G.C. Lukey, A. Palomo, J.S.J. van Deventer, "Geopolymer technology: the current state of the art", *J Mater Sci*, Vol. 42, pp. 2917-2933, 2007.

66. Dollase, W.A., "Least-squares refinement of the structure of a plutonic nepheline", *Zeitschrift fur Kristallographie*, Vol. 132, pp. 27-44, 1970.

67. Le Roux, S., V. Petkov, "ISAACS - interactive structure analysis of amorphous and crystalline systems", *J. Appl. Cryst.*, Vol. 43, pp. 181-185, 2010.

68. King, S.V., "Ring configurations in a random network model of vitreous silica", *Nature*, Vol. 213, pp. 1112-1113, 1967.

69. Zoltai, T., "Classification of silicates and other minerals with tetrahedral structures", *American Mineralogist*, Vol. 45, pp. 960-973, 1960.

70. Papike, J.J., M. Cameron, "Crystal chemistry of silicate minerals of geophysical interest", *Reviews of Geophysics and Space Physics*, Vol. 14, pp. 37-80, 1976.